NBSIR 83-1680

INTERIM PROGRESS REPORT: FRACTURE TOUGHNESS OF STEEL WELDMENTS FOR ARCTIC STRUCTURES

T. L. Anderson
H. I. McHenry

National Bureau of Standards
U.S. Department of Commerce
Boulder, Colorado 80303

December 1982

NBSIR 83-1680

INTERIM PROGRESS REPORT: FRACTURE TOUGHNESS OF STEEL WELDMENTS FOR ARCTIC STRUCTURES

T. L. Anderson
H. I. McHenry

Fracture and Deformation Divison
National Measurement Laboratory
National Bureau of Standards
U.S. Department of Commerce
Boulder, Colorado 80303

December 1982

Sponsored by
U.S. Department of Interior
Minerals Management Service
12203 Sunrise Valley Drive
Reston, Virginia 22091

U.S. DEPARTMENT OF COMMERCE, Malcolm Baldrige, Secretary

NATIONAL BUREAU OF STANDARDS, Ernest Ambler, Director

CONTENTS

		Page
1.	INTRODUCTION	1
2.	TECHNICAL APPROACH	2
3.	CURRENT FRACTURE TOUGHNESS REQUIREMENTS	3
	3.1 Pressure Vessels and Piping	4
	3.2 Ships	5
	3.3 Bridges	5
	3.4 Summary Comments	6
4.	EXPERIMENTAL PROCEDURE	6
	4.1 Test Material	6
	4.2 Tensile Tests	6
	4.3 Charpy V-Notch Impact Tests	7
	4.4 Fracture Toughness Tests	7
5.	RESULTS AND DISCUSSION	10
	5.1 Tensile Tests	10
	5.2 Charpy-Impact Data	10
	5.3 Fracture Toughness	11
	5.4 Predicting the Effect of Constraint on the Ductile-to-Brittle Transition	12
	5.5 Detecting the Onset of Tearing	13
	5.6 Estimation of J from CMOD	14
	5.7 Relationships Between J and CTOD	15
	5.8 The Eta Factor	16
6.	SUMMARY AND CONCLUSIONS	17
REFERENCES		18
APPENDIX		50

List of Figures

		Page
1.	The ductile-to-brittle transition of steel showing brittle (linear elastic), elastic-plastic, and ductile (fully plastic) regions.	31
2.	Location of Charpy V-notch specimens for weld qualification tests.	32
3.	Single-edge notched bend (SENB) specimen used to obtain fracture toughness values.	33
4.	Orientation of SENB specimens with respect to the rolling direction. Charpy impact specimens were also prepared with this orientation.	34
5.	Photograph of the test machine and three-point bend fixture.	35
6.	Notation for reporting critical CTOD values [13].	36
7.	Tensile properties of ABS grade EH36 steel as a function of temperature.	37
8.	Charpy impact transition curve for ABS grade EH36 steel.	38
9.	Critical CTOD for cleavage as a function of temperature and specimen thickness for ABS grade EH36 steel. W = 25.4 mm (1.0 in).	39
10.	Critical J for cleavage as a function of temperature and specimen thickness for ABS grade EH36 steel. W = 25.4 mm (1.0 in).	40
11.	Critical CTOD for cleavage as a function of temperature and crack length for ABS grade EH36 steel. W = 25.4 mm (1.0 in).	41
12.	Critical J for cleavage as a function of temperature and crack length for ABS grade EH36 steel. W = 25.4 mm (1.0 in).	42
13.	Critical CTOD for the onset of tearing as a function of temperature and specimen geometry for ABS grade EH36 steel. W = 25.4 mm (1.0 in).	43
14.	Critical J for the onset of tearing as a function of temperature and specimen geometry for ABS grade EH36 steel. W = 25.4 mm (1.0 in).	44
15.	Comparison of predicted and experimental CTOD values as a function of temperature and specimen thickness.	45
16.	Computer plots of the first and second derivatives of q with respect to V. A sharp drop in the first derivative generally indicates tearing.	46
17.	Comparison of J estimates from equations 8 and 9.	47
18.	The ratio of the plastic components of J and CTOD and an estimate of the plastic m factor as a function of displacement.	48
19.	The overall eta factor (η_o) as a function of a/W and displacement. The elastic eta factor curve [17] is superimposed for comparison.	49

List of Tables

		Page
1.	Charpy V-Notch Requirements for Steel Plates in OCS Platforms.	20
2.	Charpy V-Notch Requirements for Fracture-Critical Members in Arctic Bridges.	21
3.	Charpy V-Notch Requirements for Pressure Vessels and Piping.	22
4.	Chemical Composition of the ABS Grade EH36 Steel.	23
5.	Test Matrix for Fracture Toughness Tests on SENB Specimens.	23
6.	Tensile Properties of the ABS Grade EH36 Steel.	24
7.	Charpy V-Notch Impact Data for ABS Grade EH36 Steel.	25
8.	Summary of Fracture Toughness Tests on Five Geometries of SENB Specimens.	26
	a. B = 0.5 W = 12.7 mm	26
	b. B = W = 25.4 mm	27
	c. B = 15 W = 38.1mm	28
	d. B = W = 25.4 mm	29
	e. B = W = 25.4 mm	30

FRACTURE TOUGHNESS OF STEEL WELDMENTS FOR ARCTIC STRUCTURES

T. L. Anderson
H. I. McHenry

This report summarizes the progress in the development of fracture criteria for steel weldments in arctic structures. Tensile, Charpy-impact, and fracture toughness properties have been measured as a function of temperature for a 25.4 mm (1 in) thick plate of normalized steel. Fracture toughness tests were performed on five geometries of single-edge notched bend (SENB) specimens. Critical values of the J-integral and the crack-tip opening displacement (CTOD) were computed and plotted versus temperature. The ductile-to-brittle transition temperature increased with increasing specimen thickness, and crack length. The effect of specimen geometry on fracture toughness is attributed to changes in crack-tip region constraint with geometry. Initial attempts to model this behavior have been moderately successful.

Various aspects of the SENB fracture toughness test are being examined. Preliminary results indicate that the J-integral can be accurately measured with either load-line displacement or mouth-opening displacement measurements. It may therefore be possible to measure both J and CTOD with a single clip gage. The relationship between J and CTOD has been investigated. The ratio of J to CTOD is a function of yield strength, displacement and work-hardening rate. The eta factor, which is a dimensionless constant used to relate the J-integral to energy absorbed by the specimen, was found to be independent of crack length for SENB specimens with a/W ranging from 0.19 to 0.75.

Key words: arctic structures; crack-tip opening displacement; ductile-to-brittle transition; elastic-plastic fracture; J-integral; mechanical properties; structural steels; toughness.

1. INTRODUCTION

The development of oil and gas resources in the Arctic will require the construction of fixed offshore platforms capable of operating safely at temperatures of -40°C and possibly lower. The platforms are likely to be welded steel structures because of steel's relatively low cost, ease of

fabrication, high strength, and the availability of grades that are highly fracture resistant at low temperatures. The arctic environment is potentially hazardous from a structural integrity standpoint because steel weldments have increased susceptibility to brittle fracture at low temperatures. Thus, material toughness criteria are needed to ensure that steels with adequate fracture resistance at low temperatures are used to build these platforms. The objective of the present study is to develop a quantitative basis for specifying the fracture toughness of steel weldments for arctic structures.

The present report summarizes the overall program plan and the progress to date. The technical approach, which is based on elastic-plastic fracture mechanics, is summarized in the next section. A review of current code requirements for the fracture toughness of steels used in arctic structures is given in Section 2. The experimental procedures, the results and discussion, and the summary and conclusions are given in Sections 4, 5, and 6, respectively. A literature review covering the basic concepts of fracture mechanics and recent research pertinent to the present study is included as an appendix.

2. TECHNICAL APPROACH

The principles of fracture mechanics [1,2] provide the technical basis for this investigation. Fracture mechanics is the study of the influence of loading, crack size, and structural geometry on the fracture resistance of materials containing cracks. There are two main ideas in fracture mechanics. First, fracture occurs when the driving force for fracture, a function of stress and flaw size, exceeds the material's resistance to fracture, referred to as the fracture toughness. Second, fracture toughness is a geometry-independent material property; i.e., a simple laboratory specimen and a large structure both fracture at the same critical value of driving force. Both of these ideas work quite well for materials that behave in a linear elastic manner; i.e., fracture occurs prior to extensive plastic deformation. Recent progress in ductile fracture mechanics suggests that these ideas are also valid for materials that fracture in a fully ductile manner [3].

Contrary to common assumptions, there is not a geometry-independent fracture criterion for the transition region between linear elastic and fully-ductile fracture. This transition region, identified as elastic-plastic in Fig. 1, is the region of interest for steel structures at low temperatures. The geometry dependence exists because steel undergoes a ductile-to-brittle

transition as temperature is reduced. In the temperature range of the transition, different fracture mechanisms may occur depending on the extent of plastic flow near the crack tip. As plastic flow decreases, the micromode of fracture changes from ductile tearing to brittle cleavage. Plastic flow can be decreased by lowering the temperature or increasing the strain rate, both of which increase the yield strength. Plastic flow can also be limited by geometrical constraint, i.e., configurations where the surrounding elastic-material limits plastic flow near the crack tip. Constraint increases with thickness (the well-known size effect) and, in bending, with crack depth-to-thickness ratio.

The fracture behavior of steels at low temperature is studied using the principles of elastic-plastic fracture mechanics (EPFM). Both the driving force and the resistance to fracture can be expressed in terms of an EPFM parameter, either the crack tip opening displacement (CTOD) or the J-integral (J). Fracture occurs when the applied CTOD (or J) exceeds a critical value of CTOD (or J). The critical value of CTOD, denoted δ_c, or of J (J_c) is the fracture toughness of the material. Unfortunately, in the temperature range of the ductile-to-brittle transition, δ_c and J_c are not geometry independent. Thus, one of the main ideas of fracture mechanics, the applicability of laboratory fracture toughness data to practical structures, is not valid.

The approach being used to develop fracture criteria for arctic structures is based on EPFM. Fracture toughness of a C-Mn steel plate is measured as a function of geometrical constraint at temperatures throughout the ductile-to-brittle transition. Constraint is varied by changing the crack-length specimen-width ratio and the thickness of single edge notch bend (SENB) specimens. In each test, fracture toughness is measured by the two principal EPFM parameters, CTOD and J. The effect of constraint on fracture toughness is modeled in an attempt to predict the temperature shifts in the ductile-to-brittle transition curve with changes in constraint. A suitable method to account for constraint may eventually be used in conjunction with the Burdekin-Dawes [4,5] design curve to assess the fitness-for-service of steel weldments.

3. CURRENT FRACTURE TOUGHNESS REQUIREMENTS

In 1979, the United States Geological Survey published the "Requirements for Verifying the Structural Integrity of OCS Platforms" [6]. These

requirements include state-of-the-art performance standards which must be met in designing, fabricating, and installing OCS platforms, including those on ice or gravel islands in the arctic. The objective of the requirements is to ensure that offshore oil and gas platforms and other structures have a high probability of surviving the environmental and operational conditions to which they may be exposed.

To ensure satisfactory fracture resistance, the USGS provided the guidelines shown in Table 1 for specifying minimum levels of Charpy V-notch (CVN) impact toughness for low and intermediate strength steels. The CVN toughness guidelines for intermediate strength (310 to 415 MPa yield strength) steel plates is 34 J in the longitudinal orientation. The test temperature for steels in the most severe applications is 30°C below the service temperature. Testing at 30°C below the service temperature is not practical in arctic structures because economical steels with sufficient toughness at -70°C are simply not available. Thus, the requirements state: "For service temperatures less than -30°C, test temperatures (for CVN testing) should be specially considered."

The specification of an energy level and test temperature for CVN testing varies for different types of structures that are subjected to low temperatures during service. In the following subsections, the fracture criteria specified for pressure vessels and piping, ships, and bridges are reviewed.

3.1 Pressure Vessels and Piping

The toughness requirements for pressure vessels (ASME Section VIII, [7]) and piping (ANSI and B31.3 [8]) are a function of strength level, deoxidation practice, and heat treatment. Minimum CVN values for carbon and low alloy steels are specified in terms of average absorbed energy at a specified temperature as shown in Table 2. The toughness requirements for higher strength steels, steels heat treated to enhance strength, and stainless steels are specified in terms of notch ductility as measured in a CVN test, 0.38 mm (0.015 inch) lateral expansion is required. The test temperature for all grades is the design temperature or the minimum temperature at which pressure will be applied, whichever is lower. A lower test temperature must be used when subsize tests are conducted and the subsize width is less than 80% of the material thickness; e.g., the test temperature for half- and quarter-size CVN specimens are reduced by 11 and 28°C, respectively.

For welded pressure vessels, the CVN toughness of the weld metal and the heat-affected-zone (HAZ) must equal or exceed the toughness values specified for the base metal at the same (or lower) test temperature. Tests are conducted on the weld procedure qualification test plates and the production test plates. Weld metal specimens are notched perpendicular to the surface with one face of the specimen located within 1.5 mm of the surface. The HAZ specimens are etched before notching and the notch is cut approximately normal to the surface in such a manner as to include as much HAZ material as possible in the resulting fracture.

3.2 Ships

The class of ship that have service temperatures that approximate arctic conditions are the liquified natural gas (LNG) carriers. In these ships, significant portions of the hull are cooled by the cryogenic cargo to temperatures ranging from 0 to -46°C [9]. To avoid brittle fracture, the U.S. Coast Guard (USCG) [10] and the American Bureau of Shipping (ABS) [11] and comparable regulatory authorities around the world have established CVN requirements on the steels and welds subjected to low temperatures. The CVN tests are conducted at 5.5°C below the minimum service temperature. The specimens are cut transverse to the rolling direction and to the weld axis with notches normal to the plate surface. Each plate is tested and welds are tested from the weld procedure qualification plates and from the production test plates. Three specimens are tested in each of the following notch locations: base metal; centered in the weld metal; on the fusion line; and in the HAZ at 1, 3, and 5 mm from the fusion line. The impact specimen locations are summarized in Fig. 2. The average CVN value must equal or exceed 27.5 J (20 ft-lb); the minimum value for one specimen is 18.6 J (13.3 ft-lb).

3.3 Bridges

The toughness requirements for arctic bridges have been established by the American Association of State Highway Transportation Officials (AASHTO) [12]. The requirements are applicable to fracture critical members, which are defined as those tension components of a bridge whose failure would be expected to result in the collapse of the bridge. The CVN values specified are summarized in Table 3. For low and intermediate strength steels, the test temperature is 39°C above the minimum service temperature, i.e., a bridge

design for -51°C service uses steels tested at -12°C. The rationale for the test temperature being higher than the service temperature is two-fold. First, the actual loading rate in a bridge is substantially slower than the loading rate in a CVN test. The test temperature is increased by an amount equal to the shift in transition temperature as the loading rate is decreased from the impact rate used in CVN tests to the maximum loading rate expected in bridges. Second, other factors such as service experience, design and fabrication controls, and the results of fatigue tests on similar welded beams also contribute to the expectation of safe performance by the bridge.

3.4 Summary Comments

Consideration of existing fracture criteria for steel weldments used at low temperatures does not provide clear guidance for the establishment of fracture criteria applicable to fixed platforms in the Arctic. Consider, for example, the range of test temperatures required. The CVN test temperatures range from 30°C below the minimum service temperature, T_m, for OCS platforms to 39°C above T_m for arctic bridges, with intermediate requirements for ships and pressure vessels. Clearly, objective criteria are missing.

4. EXPERIMENTAL PROCEDURE

4.1 Test Material

The test material is a 25.4 mm thick plate of ABS grade EH36 steel, a 350 MPa (51 ksi) yield strength C-Mn steel. The chemical composition is given in Table 4. The steel is in the normalized condition and has particularly uniform properties due to sulfide shape control. Thus, material variability should not have an undue influence on the test results.

4.2 Tensile Tests

Round tensile specimens (6.35 mm diameter and 31.75 mm gage length) with the tensile axis parallel to the rolling direction were tested at various temperatures ranging from -196°C to 25°C. All tensile tests were performed in a screw-driven tensile test machine at a cross-head speed of 0.2 cm/min. The upper yield point, lower yield stress, ultimate tensile strength, percent reduction in area, percent elongation and true stress at fracture were measured for each test. All testing and measurement procedures conformed to the guidelines of ASTM E-8, the standard for tension testing of metals.

The testing machine is equipped with a fixture designed for cryogenic testing. Various temperatures are attained by an elaborate temperature control system. The specimen is cooled by reservoirs of liquid nitrogen above and below the specimen. The specimen grips are equipped with electric heaters which are connected to controllers. The desired temperature is simply dialed into the controllers. The combination of heating and cooling the specimen produces a steady-state temperature.

4.3 Charpy V-Notch Impact Tests

The Charpy-impact transition curve has been established for the normalized steel in the temperature range -196 to 25°C. The procedures of ASTM E-23, the standard for impact testing, were followed in most cases. Deviations from the standard occurred in some tests. These deviations are noted in the results and discussion section. For each test the absorbed energy, percent shear and lateral expansion were measured. The latter two quantities were measured according to the guidelines which appear in ASTM A-370. The maximum lateral expansion was measured with a digital micrometer.

The various test temperatures were attained by placing the specimens in a constant temperature bath (liquid nitrogen or a liquid nitrogen - methanol mixture) for a minimum of ten minutes. Each specimen was then removed from the bath and tested within five seconds.

4.4 Fracture Toughness Tests

The ductile-to-brittle transition curves have been established as a function of constraint in single-edge notched bend (SENB) specimens (see Fig. 3). Notch constraint is varied by varying the crack-length/width ratio (a/W) and the specimen thickness (B). The specimens are machined with the notch orientation shown in Fig. 4.

All specimens are fatigue-precracked at room temperature according to the specifications in the British standard for COD testing [13]. The maximum allowable stress intensity for fatigue loading, $K_f(max)$, is given by:

$$K_f(max) = 0.63\sigma_y B^{1/2} \qquad (1)$$

where σ_y is the yield strength (in MPa) and B is the specimen thickness (in mm). The British standard states that the minimum stress intensity, $K_f(min)$, be at least 10% of $K_f(max)$, so that:

$$\Delta K_f \leq 0.9\ K_f(max). \qquad (2)$$

The test matrix is shown in Table 5. For each notch configuration test temperatures cover the complete fracture mode transition, i.e., cleavage to ductile tearing.

All tests are performed in displacement control on a 100 kN servohydraulic test machine. The displacement rate in all tests is 0.80 mm/min. This corresponds to a loading rate (in the elastic range) for the square section (W = B) specimens of approximately 9.3 kN/s for shallow notched (a/W = 0.25) specimens and 375 N/s for th deep notched (a/W = 0.75) specimens. The experimental setup is shown in Fig. 5. Th mouth-opening displacement and the load-line displacement are measured simultaneousl during the test by two clip gages. The load-line displacement is measured by the comparison bar technique developed by Dawes [14]. The load and the two displacement are recorded on a two-pen X-Y plotter. The test instrumentation is wired to a mini-computer through an analog-to-digital converter. The load, crosshead displacement, both clip-gage displacements are recorded by the computer at approximately 0.3 s intervals and stored on a magnetic disk. The computer typically collects and stores around 500 sets of data in a 3 to 5 minute bend test.

Low temperatures are attained by attaching a box to the lower crosshead and filling it with either liquid nitrogen or an alcohol and dry ice mixture. Intermedi temperatures (between -196 and -70°C) can be attained by pouring liquid nitrogen int the box to a level below the specimen. The specimen is cooled by heat transfer thrc the test fixture and by the vapor coming off of the boiling nitrogen below the specimen. The actual specimen temperature is measured by a thermocouple implanted i the specimen.

In each test, fracture toughness is measured by the two EPFM parameters, J and CTOD. Figure 6 shows the notation used for critical values of CTOD. The notation depends on the nature of the fracture event, i.e. whether the crack extension is brittle or ductile, and whether or not unstable cleavage is preceded by stable crac growth. A similar notation is used for reported critical values of the J-integral.

The crack-tip opening displacement (CTOD) is computed from the following relationship:

$$\delta = \delta_e + \delta_p = \frac{K^2}{2\sigma_y E} + \frac{r_p(W-a)\, V_p}{r_p(W-a) + a + Z} \qquad (3)$$

where V_p = the plastic component of the mouth-opening displacement
Z = knife edge thickness
r_p = rotational factor.

This equation separates CTOD into elastic and plastic components (δ_e and δ_p, respectively). The British standard [13] suggests that a value of 0.4 be assumed for r_p in equation (3). However, a more precise value for the rotational factor can be calculated if the plastic components of load-line displacement and mouth-opening displacement (q_p and V_p, respectively) are known [15]:

$$r_p = \frac{1}{W-a} \frac{V_p W}{q_p} \{(1 - \frac{q_p}{16W}) - (a + z)\} \qquad (4)$$

In most cases the J-integral for an SENB specimen is estimated from the following equation

$$J = \frac{2U}{B(W-a)} \qquad (5)$$

where U is the area under the load/load-line displacement curve. In some cases other J-estimation procedures are used and the results from the various procedures are compared. The details of those procedures are given in the results and discussion.

The method that is utilized to detect the onset of stable crack growth is the double displacement method. Both the mouth-opening displacements, V, and the load-line displacements, q, from each test are stored on a magnetic disk. A program has been written which computes dq/dV and d^2q/dV^2, and plots them as a function of V. The critical displacement is inferred from these plots.

5. RESULTS AND DISCUSSION

5.1 Tensile Tests

The tensile properties have been obtained for 10 temperatures ranging from -196°C to 25°C. These data are shown in Fig. 7 and in Table 6. The data follow the expected trends with a minimal amount of scatter. Both the yield strength and the ultimate tensile strength increase markedly with decreasing temperature. All flow curves exhibited an upper and lower yield point which is characteristic of low-carbon steels. The yield strength (as plotted in Fig. 7) was defined as the upper yield point.

5.2 Charpy-Impact Data

The Charpy V-notch impact energy transition curve has been established and is shown in Fig. 8. The percent shear and lateral expansion were also measured for each specimen. The Charpy data are summarized in Table 7. Figure 8 shows that the ductile-to-brittle transition occurs at about -70°C. Note that the curve is nearly vertical at this temperature. Most specimens tested at or near this temperature exhibited either fully brittle (low energy) or fully ductile (high energy) behavior. Only a few specimens exhibited intermediate behavior. Table 7 shows that the transition from low energy to high absorbed energy corresponds well with the fracture surface transition (0% shear to 100% shear) and the transition from small to large lateral expansion.

Because of the high toughness of this material, most of the upper shelf energy values are invalid according to the ASTM E-23 standard. The full-scale energy of the charpy test machine used in this experiment is 358 J. According to the ASTM standard the energy absorbed by an impact specimen should not exceed 80% of the full-scale energy of the test machine. Therefore, all energy values above 268 J do not meet the requirements of ASTM E-23.

Figure 8 illustrates an inherent weakness of material toughness requirements based on Charpy data. For example, if the service temperature is -40°C the required toughness based on present OCS platform requirements would be 34 J at -70°C. At this temperature there is a drastic drop in toughness to well below 34 J while at the service temperature (-40°C) the material is fully ductile and has a toughness of greater than 250 J.

5.3 Fracture Toughness

The fracture toughness data which have been collected to date are summarized in Figs. 9-14 and Table 8. The critical values of J and CTOD along with the critical fracture event for each specimen is shown on these figures. Three critical fracture events have been observed. J_c and δ_c are defined at the occurrence of unstable cleavage without prior stable crack growth. J_i and δ_i are defined at the onset of stable crack growth. When cleavage is preceded by stable crack growth J_u and δ_u are measured at the point of instability.

Figures 9 and 10 show that the ductile-to-brittle transition curves shift approximately 30°C as the specimen thickness increases from 13 to 38 mm. The thickest specimen produces the highest amount of crack-tip-region constraint; constraint is the restriction of plastic flow by the surrounding elastic material. Constraint causes a triaxial stress state and raises the flow stress near the crack tip. This increase in flow stress tends to promote cleavage fracture (i.e., shift the transition curve to the right) since it is easier to reach the fracture stress.

It should be noted that the thickest specimens (B = 38.1 mm) had slightly deeper cracks than the other two specimen geometries shown in Figs. 9 and 10. The deeper cracks were necessary in order to prevent the load on the thick specimens from exceeding the capacity of the test machine. These deeper cracks, however, probably contributed in part to the shift in the transition curve to higher temperatures.

The influence of crack length on the ductile-to-brittle transition curve is shown in Figs. 11 and 12. In SENB specimens constraint increases with crack length because of the plasticity reversal (tension to compression) that must occur within the remaining ligament. Therefore the transition temperature increases with crack length. Since the crack tip in a shallow-notched specimen is near a free surface, constraint can be further relaxed by plastic flow to the free surface. The data for the deep-notched geometry ($a/W \sim 0.75$) behave in a somewhat unusual manner. The curve fitted to these data (Figs. 11 and 12) crosses the curve representing the $a/W \sim 0.5$ data. At low values of δ_c and J_c, where the plastic zone is relatively small, the deep-notched geometry has more constraint than the $a/W \sim 0.5$ geometry. At higher temperatures (and higher δ_c and J_c values) the plastic zone at fracture is on the order of the size of the ligament in the deep-notched geometry. The constraint is relaxed as the plastic zone approaches a free surface.

Figures 13 and 14 show values of δ_i and J_i, respectively, for all five specimen geometries. Both J_i and δ_i are apparently independent of geometry and δ_i is approximately independent of temperature. J_i increases slightly with decreasing temperature because the area under a load-displacement curve at a constant displacement increases with increasing flow stress. Since the material used for this study has a high tearing modulus (dJ/da) the point of incipient crack growth is not well defined, contributing to the scatter seen in Figs. 13 and 14.

Since increasing strain rate elevates the flow stess, strain rate should have an effect on the ductile-to-brittle transition. This effect is seen when the Charpy-impact transition curve in Fig. 8 is compared to the curves in Figs. 9-12. The ductile-to-brittle transition in the Charpy test (high strain rate) occurs at about -70°C while all curves in Figs. 9-12 for fracture toughness tests (low strain rate) lie to the left of this temperature. Also, note that the transition in the Charpy-impact data is much steeper than the transition in the fracture toughness data.

Figures 9-12 illustrate a problem facing the field of fracture mechanics. While the fracture behavior of a steel can be adequately described in terms of K_{Ic} on the lower shelf and J_{Ic} and R-curve analysis on the upper shelf, there is at present no fracture toughness parameter applicable to the ductile-to-brittle transition region. The fracture toughness of a material at a given temperature in the transition region is dependent on the geometry of the test specimen.

5.4 Predicting the Effect of Constraint on the Ductile-to-Brittle Transition

The limit load, P_L, or load at net-section yield is related to the yield stress by the following expression:

$$P_L = \frac{L\,\sigma_Y (W-a)^2 B}{4W} \qquad (6)$$

where L is a dimensionless parameter which is a measure of the constraint due to the notch. For the material used in this investigation: L = 1.38 for B = 12.7 mm, a/W = 0.2 and L = 1.52 for B = 38.1 mm, a/W = 0.29.

The quantity $L\sigma_Y$ is a measure of the average stress in the ligament at net-section yield. Thus, the ligament stress at fracture, $L\sigma_c$, can be computed as follows:

$$L\sigma_c = \frac{4P_c W}{B(W-a)^2} \tag{7}$$

where P_c is the load at fracture. The quantity $L\sigma_c$ was found to be relatively insensitive to temperature and specimen geometry. The average value of $L\sigma_c$ is 750 MPa for the material used in this study.

A simple model which assumes that $L\sigma_c$ is independent of temperature and geometry can be used to predict the effect of constraint on ductile-to-brittle transition curves. If L is known for a given geometry, the corresponding value of σ_c (the ligament stress in the absence of triaxiality) can be computed. The strain required to reach a stress of σ_c in a uniaxial tension test at a given temperature can be infered from the flow curve at that temperature. CTOD can be infered from ligament strain. It is then possible to plot δ_c as a function of temperature and L.

The above approach was applied to the three shallow-notched geometries. The resulting curves are plotted in Fig. 15 along with the experimental data. Although the shape and position of the predicted curves do not agree with experiment, the relative temperature shifts between geometries was accurately modeled by this approach.

5.5 Detecting the Onset of Tearing

During a fracture test the load-line displacement (q) is plotted autographically against the crack mouth-opening displacement (V). After net-section yield the q versus V plot yields a nearly straight line. However, as the crack grows this line gradually decreases in slope because the center of rotation moves during crack growth. Figure 16 shows a computer plot of the first and second derivatives of q with respect to V. The first derivative plot has proved to be the more useful in detecting crack growth. The behavior at the far left of this plot represents the transition from elastic to plastic deformation. During plastic deformation the first derivative remains relatively constant and then increases sharply. This increase is possibly

associated with crack-tip blunting. At V = 1.48 mm there is a sharp drop in the first derivative. This is taken as the point of incipient tearing. At higher displacements the curve has a zig-zag shape. This is believed to be associated with successive increments of tearing followed by blunting.

5.6 Estimation of J from CMOD

For deep-notched SENB specimens the J-integral is usually estimated from the following equation:

$$J = \frac{2U_T}{B(W-a)} \tag{8}$$

where U_T is the total area under the load versus load-line displacement curve. The value of J can also be estimated from the load versus mouth-opening displacement curve using equation

$$J = \frac{K^2}{E'} + \frac{2U_p^v}{B(W-a)} \left(\frac{W}{r_p(W-a)+a+z}\right) \tag{9}$$

where U_p^v is the plastic component of the area under the P/V curve. Equation 9 is based on the Sumpter and Turner [16] equation, although they approximated the area by

$$U_p^v \cong P_L V_p \tag{10}$$

where P_L is the limit load.

The J-integral has been calculated for a number of tests using equations 8 and 9 and the agreement is very good. Figure 17 shows a comparison of estimates from the two equations. The data represent a single specimen at various displacements. The difference between the two J estimates for this particular specimen range from 0.5% to 1.5%.

The value of r_p used in equation 9 to generate Fig. 17 was measured from the same specimen using equation 4. The excellent agreement between equations 8 and 9 as shown in Fig. 17 is evidence that the simple hinge mechanism is an adequate model to describe the plastic deformation of an SENB specimen. Figure 17 also shows that the J-integral can be accurately measured

from the mouth-opening displacement if r_p is known. Thus, it is possible to measure both J and CTOD from an SENB specimen with a single clip gage.

5.7 Relationships Between J and CTOD

Under conditions of small-scale yielding the relationship between J and CTOD can be estimated by:

$$J = m \sigma_Y \delta \tag{11}$$

where m = 1 for plane stress and m = 2 for plane strain [16]. The value of m for large-scale yielding should lie between 1.0 and 2.0.

The plastic term in equation 9 is similar to the equation for the plastic CTOD:

$$\delta_p = \frac{r_p(W-a)V_p}{r_p(W-a)+a+z} \tag{12}$$

From equations 9 and 12 one can obtain a simple equation for the ratio of the plastic J to the plastic CTOD

$$\frac{J_p}{\delta_p} = \frac{2U_p^v W}{V_p B r_p (W-a)^2} \tag{13}$$

The flow stress can be estimated from the limit-load expression

$$\sigma_{flow} \cong \frac{P}{(W-a)^2} \cdot \frac{4W}{1.5B} \quad (P \geq P_L) \tag{14}$$

Hence m_p can be calculated:

$$m_p = \frac{.75U_p^v}{PV_p} \tag{15}$$

Equations 13 and 15 have been incorporated into a computer program which plots J_p/δ_p and m_p as a function of displacement. A typical set of plots is

shown in Fig. 18. The ratio J_p/δ_p increases with displacement due to work hardening. Also m_p is not constant; it decreases with displacement until it levels off at a value of 1.27. Apparently the relationship between J and CTOD is more complicated than has been traditionally assumed. This may have ramifications with respect to the merits of each as a fracture characterizing parameter.

5.8 The Eta Factor

A more general form of equation 8 is:

$$J = \frac{\eta U}{B(W-a)} \tag{16}$$

where $\eta \cong 2$ for deep notched SENB specimens. The above equation can be divided into elastic and plastic components [16]:

$$J = \frac{\eta_e U_e}{B(W-a)} + \frac{\eta_p U_p}{B(W-a)} = \frac{K}{E'} + \frac{\eta_p U_p}{B(W-a)} \tag{17}$$

The elastic eta factor, η_e, can be derived from the elastic compliance and stress intensity coefficient. The solid line in Fig. 19 is a plot of η_e versus notch depth [17].

Since J is defined as the negative of the spatial derivative of work, the plastic eta factor, η_p, and the over-all eta factor, η_o, can be computed as follows:

$$J = \frac{\eta_o U}{B(W-a)} = \frac{-1}{B}\frac{dU}{da} \tag{18}$$

hence

$$\eta_o = -\frac{(W-a)}{U}\frac{dU}{da} \tag{19}$$

A series of SENB specimens with notch depths ranging from a/W = 0.19 to 0.75 were tested at room temperature. The area under the load versus load-line displacement curve, U, was measured for each specimen at displacements of 1.0, 1.5, and 2.0 mm. These values of U were then plotted versus crack length

and dU/da was measured for various crack lengths by drawing tangents to the U versus a curves and computing the slopes. The over-all eta factor, η_o, was then computed as a function of crack length. The results are plotted in Fig. 19. According to Fig. 19, η_o is relatively independent of crack length down to a/W = 0.19. It therefore seems reasonable to use a value of η = 1.8-2.0 for all J measurements from SENB specimens with a/W $\geq$ 0.2.

6. SUMMARY AND CONCLUSIONS

The existing material toughness requirements based on Charpy-impact data are somewhat inadequate. The goal of this program is to develop a fracture mechanics rationale for specifying material toughness requirements. This study, to date, has been devoted to an assessment of the base-metal fracture properties. Fracture toughness tests on weldments are planned for the immediate future.

Tensile, Charpy-impact and fracture toughness tests have been performed on ABS Grade EH36 steel over a wide range of temperatures (-196 to 25°C). The Charpy-impact transition curve is nearly vertical at approximately -70°C. The upper-shelf energy of this material is very high ($\sim$330 J). Critical values of J and CTOD were measured for five geometries of SENB specimens. The ductile-to-brittle transition curves for the SENB tests are much less steep than the Charpy data; the transition temperatures for the fracture toughness tests are all lower than that for the Charpy data. Specimen geometry has a drastic effect on fracture toughness in the transition region. Increasing specimen thickness and/or crack length markedly increases the transition temperature. Larger specimens produce a greater amount of stress triaxiality near the crack tip, thus elevating the flow stress locally. A higher flow stress tends to promote cleavage fracture since it is easier to reach the fracture stress. Since fracture toughness in the transition region is geometry dependent, one cannot safely predict the fracture behavior of a large structure from the toughness of a small, laboratory specimen.

Initial attempts to model the effect of constraint on fracture toughness have been moderately successful. It is possible to predict the temperature shifts (due to constraint) in ductile-to-brittle transition curves with the existing model. Further refinements of the model are needed to accurately predict the position and shape of transition curves.

Preliminary data suggest that it is possible to measure both J and CTOD with a single clip gage which measures the mouth-opening displacement. It was also found that the ratio between J and CTOD is a function of displacement, yield strength, and work-hardening rate. Direct experimental measurement of the eta factor, a dimensionless constant used in J calculations, show that it is approximately equal to 1.85 for displacements of up to 2.0 mm and a/W ranging from 0.19 to 0.75.

REFERENCES

[1] Broek, D., "Elementary Engineering Fracture Mechanics," Noordhoff International Publishing, Leyden, The Netherlands (1974).

[2] Rolfe, S. T. and Barsom, J. M., "Fracture and Fatigue Control in Structures, Applications of Fracture Mechanics," Prentice-Hall, Englewood Cliffs, New Jersey (1977).

[3] Larson, L. H., Editor, "Advances in Elasto-Plastic Fracture Mechanics," Applied Science Publishers, London (1980).

[4] Burdekin, F. M. and Dawes, M. G., "Practical Use of Yielding and Linear Elastic Fracture Mechanics With Particular Reference to Pressure Vessels," Institute of Mechanical Engineers Conference on "Practical Applications of Fracture Mechanics to Pressure Vessel Technology," London, (May 1971).

[5] Anon., "Guidance on Some Methods for the Derivation of Acceptance Levels for Defects in Fusion Welded Joints," PD6493:1980, British Standards Institution, London (1980).

[6] Anon., "Requirements for Verifying the Structural Integrity of OCS Platforms," U.S. Geological Survey, Reston, VA (Oct. 1979).

[7] Anon., "ASME Boiler and Pressure Vessel Code, Section VIII, Pressure Vessels," American Society for Mechanical Engineers, New York, NY (1977).

[8] Anon., "Chemical Plant and Petroleum Refining Piping," ANSI B31.3, American Society for Mechanical Engineers, New York, NY (1977).

[9] McHenry, H. I., "Ship Steel Weldments for Low Temperature Service," Welding Journal, 55(5), 1975, pp. 387-393.

[10] Anon., U.S. Coast Guard Marine Engineering Regulations, Subchapter F, CG-115, U.S. Coast Guard, Washington, DC (July 1970).

[11] Anon., Rules for Building and Classing Steel Vessels, American Bureau of Shipping, New York, NY (1974).

[12] Anon., Standard Specifications for Highway Bridges, American Association of State Highway and Transportation Officials, Washington, DC, 12th Edition, (1977).

[13] British Standard 5762: Methods for Crack Opening Displacement (COD) Testing, 1979, The British Standards Institution, London.

[14] Dawes, M. G., "Displacements and Rotational Factors in SENB specimens." The Welding Institute Research Bulletin, 7, 1976, p. 185.

[15] Lin, I. H., Dawes, M. G., deWit, R., and Anderson, T. L., "Displacements and Rotational Factors in Single Edge Notched Bend Specimens". Submitted for publication to the International Journal for Fracture.

[16] Dawes, M. G., "Elastic-Plastic Fracture Toughness Based on the COD and J-Contour Integral Concepts". In ASTM STP 668, 1979, p. 307.

[17] Sumpter, J. D. G. and Turner, C. E., "A Method for Laboratory Determination of J_c". In ASTM STP 601, 1976, p. 3.

[18] Towers, O. L., "Stress Intensity Factors, Compliances and Elastic η Factors for Six Test Geometries." Welding Institute Report 7709.01.81/249.1, 1981.

Table 1. Charpy V-Notch Requirements for Steel Plates in OCS Platforms

GRADE	Section Size, T mm	CVN Energy* Joules (ft lb)		Test Temperature*		
		Longitudinal	Transverse	Category a	Category b	Category c
I(σ_Y < 310 MPa)	6 < T $\leq$ 38	20 (15)	20 (15)	30°C < T_m	10°C < T_m	T_m
I	> 38	25 (20)	20 (15)	30°C < T_m	10°C < T_m	T_m
II(310 < σ_Y < 415 MPa)	> 6	34 (25)	23 (17)	30°C < T_m	10°C < T_m	T_m
III(415 < σ_Y < 690 MPa)	Special consideration					

*T_m = minimum service temperature

Category a: For structural members and joint cans which are fracture critical, which experience an unusually detrimental combination of stress concentration, rapid loading, cold working, restraint and thickness, the impact test guidelines of Table 1 should be met at test temperatures to -30°C. For service temperatures below -30°C, test temperatures should be specially considered.

Category b: For structural members and joint cans which are to sustain significant tensile stress and whose fracture would pose a threat to the survival of the structure.

Category c: For primary structural members subjected to significant tensile stresses and whose usage warrants impact toughness testing.

Category d: For structural members which are sufficiently structurally redundant so that their fracture would not pose a threat to the survivability of the structure, the toughness criteria specified for (c) above may be replaced by a demonstration that the materials used in such cases are appropriate for the loading conditions, loading rates, and temperatures encountered in service.

Table 2. Charpy V-notch Requirements for Fracture-Critical Members in Arctic Bridges*

ASTM Designation	Thickness, inches	Required Toughness (J) ft-lb
A36	Up to 102 mm (4 in)	(34) 25 at 10°F (-12°C)
A572	Up to 102 mm (4 in) mechanically fastened	(34) 25 at 10°F (-12°C)
A572	Up to 51 mm (2 in) welded	(34) 25 at 10°F (-12°C)
A588	Up to 102 mm (4 in) mechanically fastened	(34) 25 at 10°F (-12°C)
A588	Up to 51 mm (2 in) welded	(34) 25 at 10°F (-12°C)
A588	Over 51 mm to 102 mm (2-4 in) welded	(41) 30 at 10°F (-12°C)
A514	Up to 102 mm (4 in) mechanically fastened	(48) 35 at -30°F (-34°C)
A514	Up to 64 mm (2.5 to 4 in) welded	(48) 35 at -30°F (-34°C)
A514	Over 64 mm to 102 mm (2.5 to 4 in) welded	NOT PERMITTED

*Non -SI units are listed first in Tables 2 & 3 in order to be consistent with the original regulatory documents [7,8,12].

Table 3. Charpy V-Notch Requirements for Pressure Vessels and Piping

Specified Minimum Tensile Strength σ_{ts}	Charpy Impact Energy, ft lb (J)			
	Killed Steels		Other Steels	
	Ave	Min	Ave	Min
Carbon and low alloy steels				
$\sigma_{ts} \leq$ 65 ksi (448 MPa)	13 (18)	10 (14)	10 (14)	7 (10)
65 (448 MPa) < σ_{ts} < 75 ksi (517 MPa)	15 (20)	12 (16)	13 (18)	10 (14)
75 (517 MPa) < σ_{ts} < 95 ksi (655 MPa)	20 (27)	15 (20)	--	--
$\sigma_{ts} \geq$ 95 ksi (655 MPa)	Lateral Expansion, inch (mm)			
	0.015 (3.8)			

Table 4. Chemical Composition of the ABS Grade EH36 Steel
(Weight Percent)

C	Mn	P	S	Si	Cu	Ni	Cr	Mo	Fe
0.12	1.39	0.015	0.006	0.380	0.05	0.03	0.05	0.007	bal.

Table 5. Test Matrix for Fracture Toughness Tests on SENB Specimens

	B = 12.7 mm	B = 25.4 mm	B = 38.1 mm
a/W = 0.2	X	X	X
a/W = 0.5		X	
a/W = 0.75		X	

W = 25.4 mm (1.0 in)

Table 6. Tensile Properties of the ABS Grade EH36 Steel

Specimen No.	Test Temp. (°C)	Upper Yield Point (MPa)	Lower Yield Stress (MPa)	Ultimate Tensile Stength (MPa)	Fracture Stress (MPa)	Percent Elongation	Percent Reduction in area
1	25	331	326	497	1313	39.7	78.2
2	25	330	325	494	1179	38.5	76.9
3	-196	843	784	888	1118	33.1	26.5
4	-160	668	625	734	1272	42.8	64.3
5	-112	617	529	668	1404	45.9	70.5
6	-80	477	419	592	1178	44.5	71.0
7	-35	414	368	548	1206	42.1	74.9
8	-174	748	680	783	1273	36.6	60.3
9	-101	498	453	619	1227	44.8	71.6
10	-139	619	543	672	1299	44.5	69.4
11	-57	403	387	565	1238	37.2	74.0
12	-17	374	363	539	1349	40.7	78.1

Table 7. Charpy V-Notch Impact Data for ABS Grade EH36 Steel

Specimen No.	Temp (°C)	Absorbed Energy (J)	Lateral Expansion (mm)	Percent Shear
1	25	336*†	2.500	100
2	25	355*†	2.220	100
3	0	355*†	2.285	100
4	-190	1	0.041	0
5	-125	4	0.055	0
6	-95	11	0.145	0
7	-70	57	0.859	3
8	-49	323*	1.630	100
9	-63	334*	1.890	100
10	-73	315*†	2.293	100
11	-80	9	0.170	0
12	-73	315*	1.843	100
13	-82	323*	1.800	100
14	-93	106	1.565	10
15	-85	22	0.345	0
16	-75	225	2.395	55
17	-76	20	0.342	0
18	-71	233	2.264	58
19	-75	355*	1.483	100
20	-75	41	0.186	0

* - Exceeds 80% of the full-scale energy

† - Specimen did not fracture completely

Table 8. Summary of Fracture Toughness Tests on Five Geometries of SENB Specimens

Table 8a. B = 0.5 W = 12.7 mm

Specimen No.	Test Temp (°C)	a/W	Critical CTOD (mm)	Critical J ($N\text{-}mm^{-1}$)
A-3	-196	.201	δ_c = 0.004	J_c = 7.1
A-17	-146	.217	δ_c = 0.050	J_c = 47
A-10	-140	.156	δ_c = 0.101	J_c = 89
A-8	-133	.190	δ_c = 0.260	J_c = 203
A-16	-125	.209	δ_c = 0.127	J_c = 99
A-19	-120	.224	δ_c = 0.308	J_c = 236
A-13	-116	.182	δ_c = 0.507	J_c = 360
A-9	-112	.178	δ_c = 0.465	J_c = 291
A-15	-112	.192	δ_u = 0.604	J_u = 421
A-18	-105	.211	δ_u = 1.33	J_u = 941
A-4	-98	.212	δ_i = 0.414	J_i = 271
			δ_u = 0.812	J_u = 547
A-14	-95	.194	δ_i = 0.603	J_i = 395
			δ_u = 1.94	J_u = 1356
A-6	-46	.219	δ_i = 0.450	J_i = 244

Table 8b. B = W = 25.4 mm

Specimen No.	Test Temp (°C)	a/W	Critical CTOD (mm)	Critical J ($N\text{-}mm^{-1}$)
B-9	-196	.218	δ_c = 0.004	J_c = 7.2
B-19	-138	.231	δ_c = 0.068	J_c = 67
B-10	-130	.206	δ_c = 0.101	J_c = 83
B-18	-120	.241	δ_c = 0.146	J_c = 114
B-11	-110	.216	δ_c = 0.371	J_c = 272
B-12	-103	.225	δ_c = 0.167	J_c = 125
B-20	-100	.228	δ_u = 0.736	J_u = 535
B-16	-89	.200	δ_u = 0.672	J_u = 461
B-14	-76	.174	δ_i = 0.550	J_i = 374
			δ_u = 2.87	J_u = 2144
B-2	-70	.208	δ_i = 0.550	J_i = 334
B-15	-67	.203	δ_i = 0.770	J_i = 475
B-1	25	.191	δ_i = 0.481	J_i = 241

Table 8c. B = 1.5 W = 38.1 mm

Specimen No.	Test Temp (°C)	a/W	Critical CTOD (mm)	Critical J ($N\text{-}mm^{-1}$)
C-2	-196	.292	δ_c = 0.004	J_c = 6.6
C-5	-137	.294	δ_c = 0.022	J_c = 27
C-15	-124	.282	δ_c = 0.141	J_c = 123
C-14	-119	.277	δ_c = 0.195	J_c = 161
C-10	-116	.276	δ_c = 0.110	J_c = 86
C-12	-112	.286	δ_c = 0.081	J_c = 70
C-11	-106	.297	δ_c = 0.210	J_c = 158
C-4	-102	.285	δ_c = 0.236	J_c = 170
C-9	-102	.289	δ_c = 0.241	J_c = 179
C-7	-96	.284	δ_c = 0.342	J_c = 247
C-13	-91	.284	δ_u = 0.750	J_u = 512
C-8	-83	.272	δ_i = 0.436	J_i = 296
C-1	25	.293	δ_i = 0.690	J_i = 403

Table 8d. B = W = 25.4 mm

Specimen No.	Test Temp (°C)	a/W	Critical CTOD (mm)	Critical J ($N\text{-}mm^{-1}$)
D-1	-196	.512	δ_c = 0.003	J_c = 5
D-14	-133	.518	δ_c = 0.047	J_c = 41
D-12	-117	.530	δ_c = 0.103	J_c = 86
D-7	-113	.542	δ_c = 0.142	J_c = 119
D-3	-108	.549	δ_c = 0.253	J_c = 201
D-19	-100	.537	δ_c = 0.306	J_c = 240
D-13	-96	.521	δ_c = 0.341	J_c = 239
D-20	-95	.533	δ_c = 0.533	J_c = 407
D-21	-91	.547	δ_c = 0.346	J_c = 259
D-17	-91	.523	δ_i = 0.500	J_i = 374
			δ_u = 0.645	J_u = 489
D-22	-85	.549	δ_c = 0.239	J_c = 171
D-8	-85	.529	δ_c = 0.275	J_c = 190
D-18	-83	.519	δ_i = 0.501	J_i = 355
			δ_u = 0.557	J_u = 411
D-16	-69	.527	δ_c = 0.390	J_c = 269
D-5	-35	.520	δ_i = 0.463	J_i = 279
D-2	25	.532	δ_i = 0.469	J_i = 259

Table 8e. B = W = 25.4 mm

Specimen No.	Test Temp (°C)	a/W	Critical CTOD (mm)	Critical J ($N\text{-}mm^{-1}$)
E-2	-196	.739	$\delta_c = 0.004$	$J_c = 6$
E-13	-121	.764	$\delta_c = 0.023$	$J_c = 22$
E-12	-115	.759	$\delta_c = 0.082$	$J_c = 79$
E-5	-104	.780	$\delta_c = 0.147$	$J_c = 121$
E-11	-102	.755	$\delta_c = 0.147$	$J_c = 125$
E-16	-101	.782	$\delta_c = 0.235$	$J_c = 206$
E-9	-95	.759	$\delta_c = 0.358$	$J_c = 336$
E-14	-91	.770	$\delta_u = 0.437$	$J_u = 368$
E-7	-83	.755	$\delta_i = 0.390$	$J_i = 331$
E-3	-52	.739	$\delta_i = 0.501$	$J_i = 343$
E-1	25	.743	$\delta_i = 0.440$	$J_i = 294$

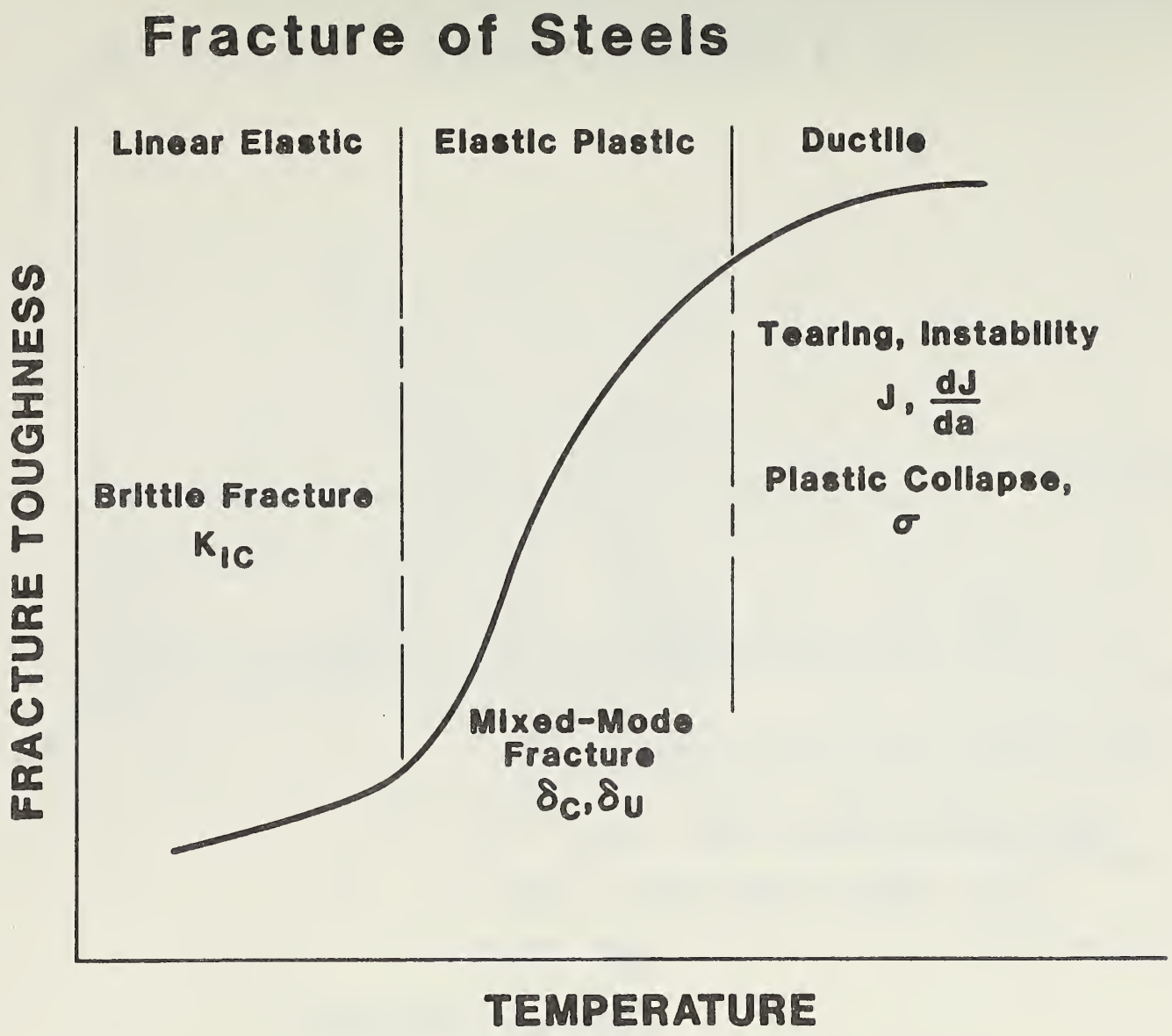

Figure 1. The ductile-to-brittle transition of steel showing brittle (linear elastic), elastic-plastic, and ductile (fully plastic) regions.

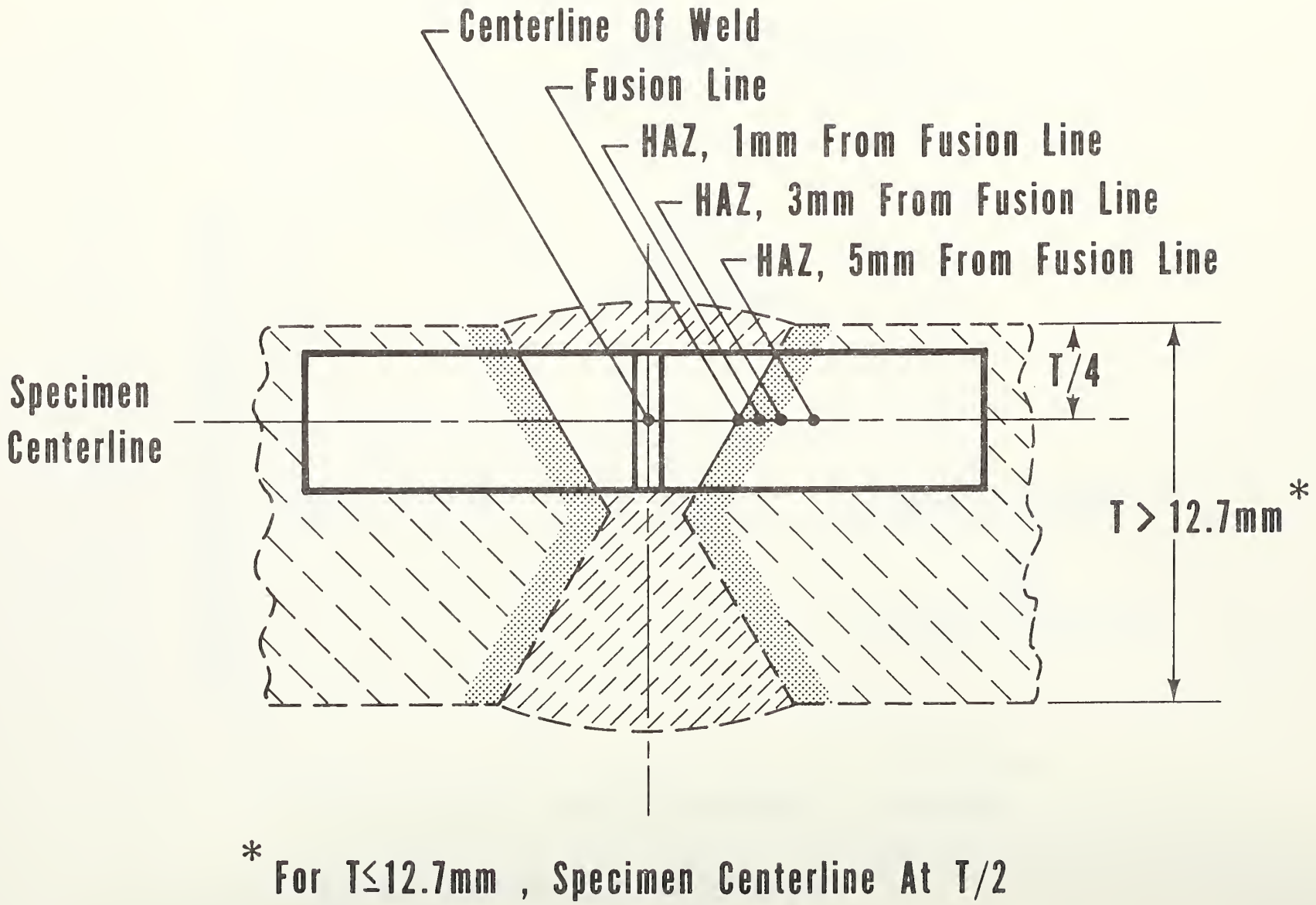

Figure 2. Location of Charpy V-notch specimens for weld qualification tests.

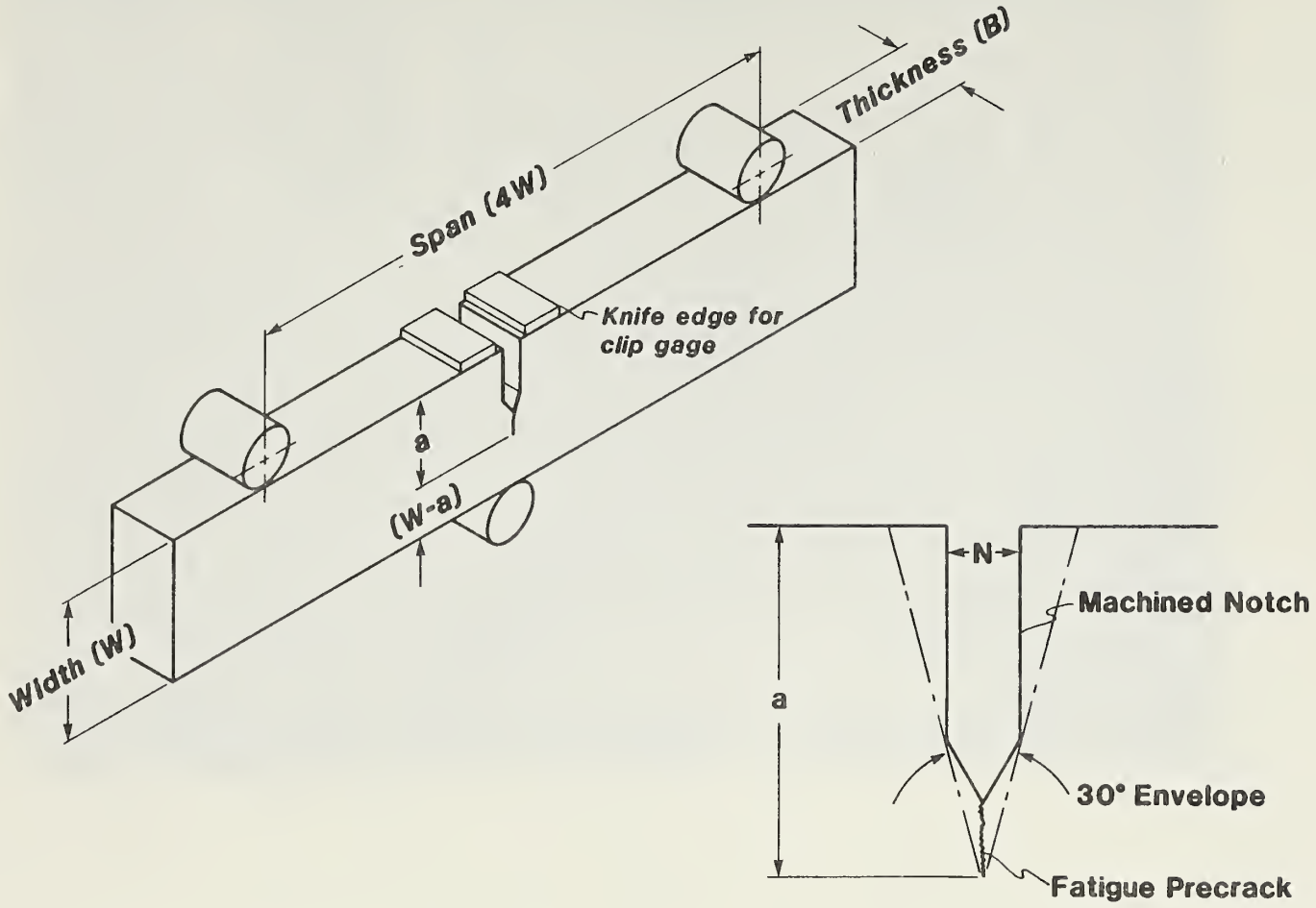

Figure 3. Single-edge notched bend (SENB) specimen used to obtain fracture toughness values.

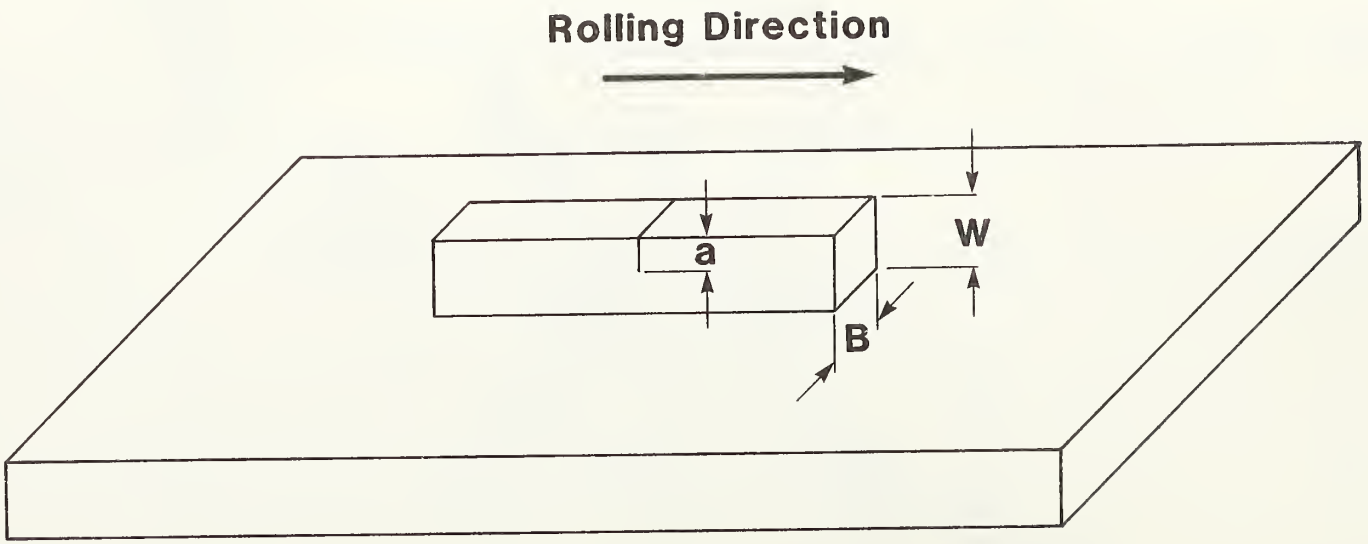

Figure 4. Orientation of SENB specimens with respect to the rolling direction. Charpy impact specimens were also prepared with this orientation.

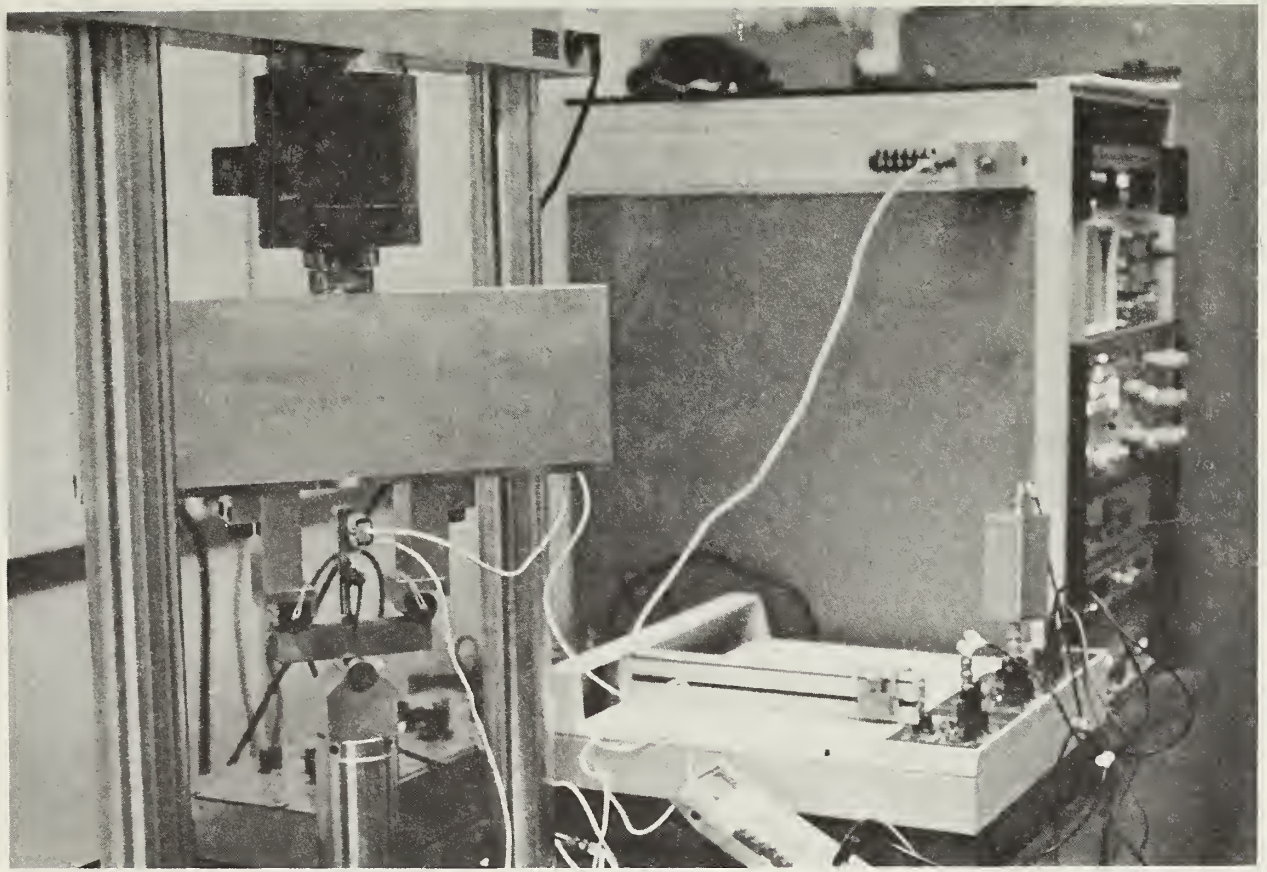

Figure 5. Photograph of the test machine and three-point bend fixture.

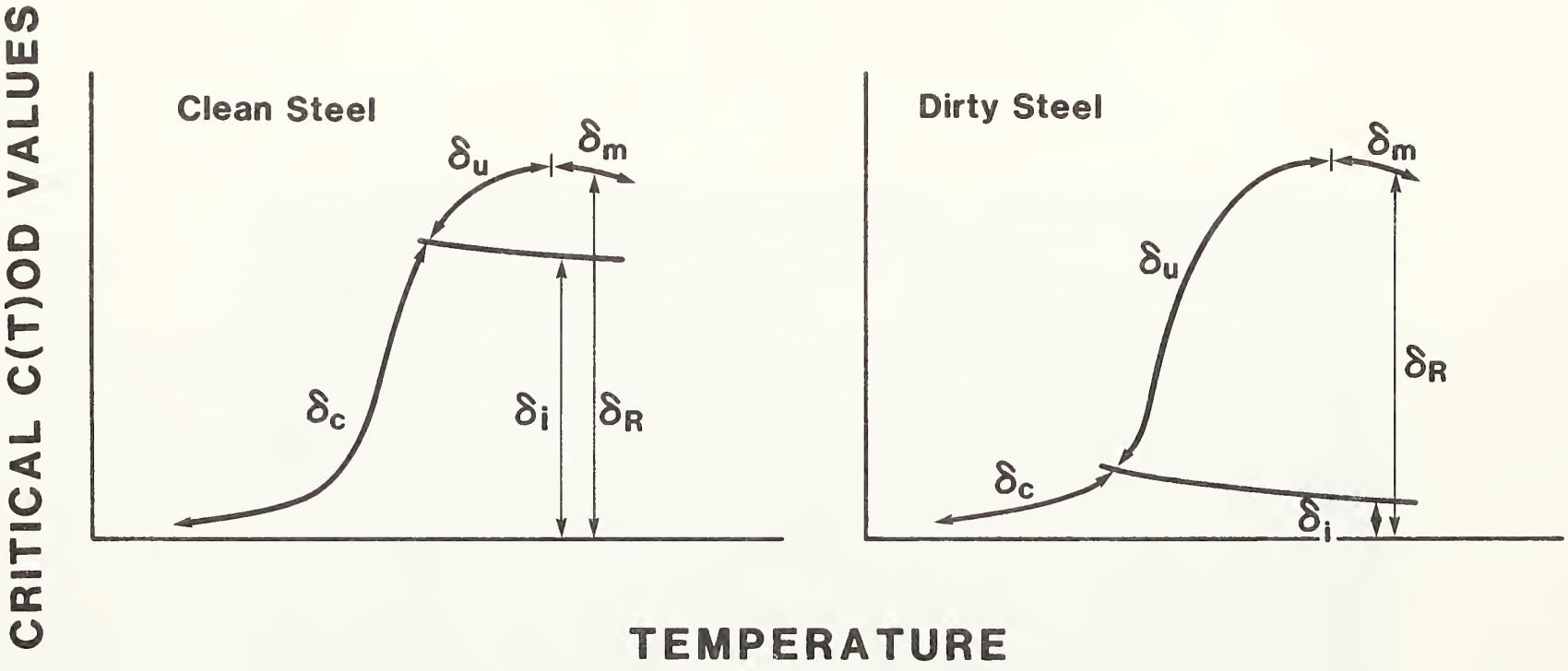

δ_c = Unstable cleavage-no prior slow crack growth

δ_u = Unstable cleavage-with prior slow crack growth

δ_m = Plastic collapse or tearing instability

δ_i = Onset of slow stable crack growth

δ_R = Resistance curve value

Figure 6. Notation for reporting critical CTOD values [13].

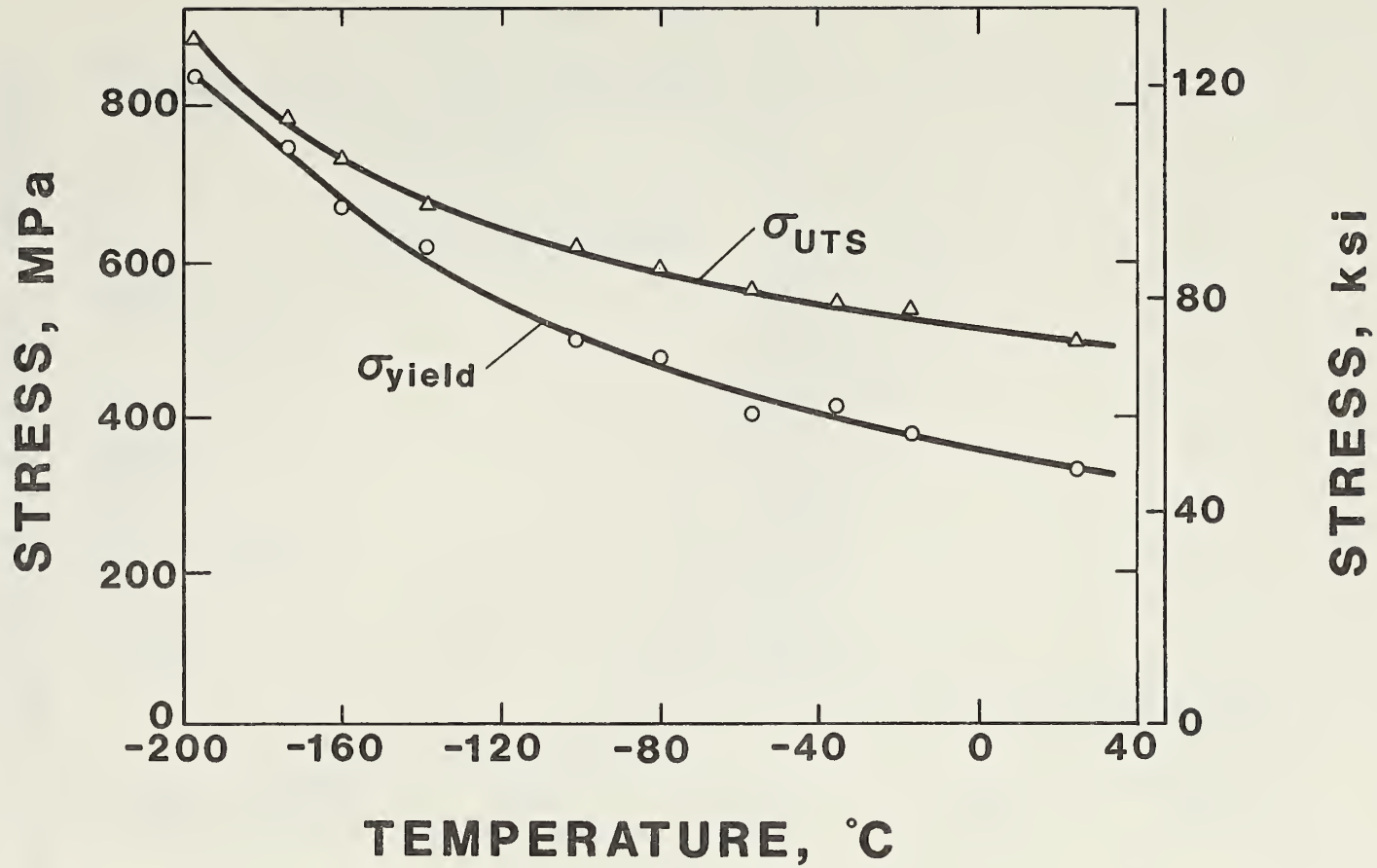

Figure 7. Tensile properties of ABS grade EH36 steel as a function of temperature.

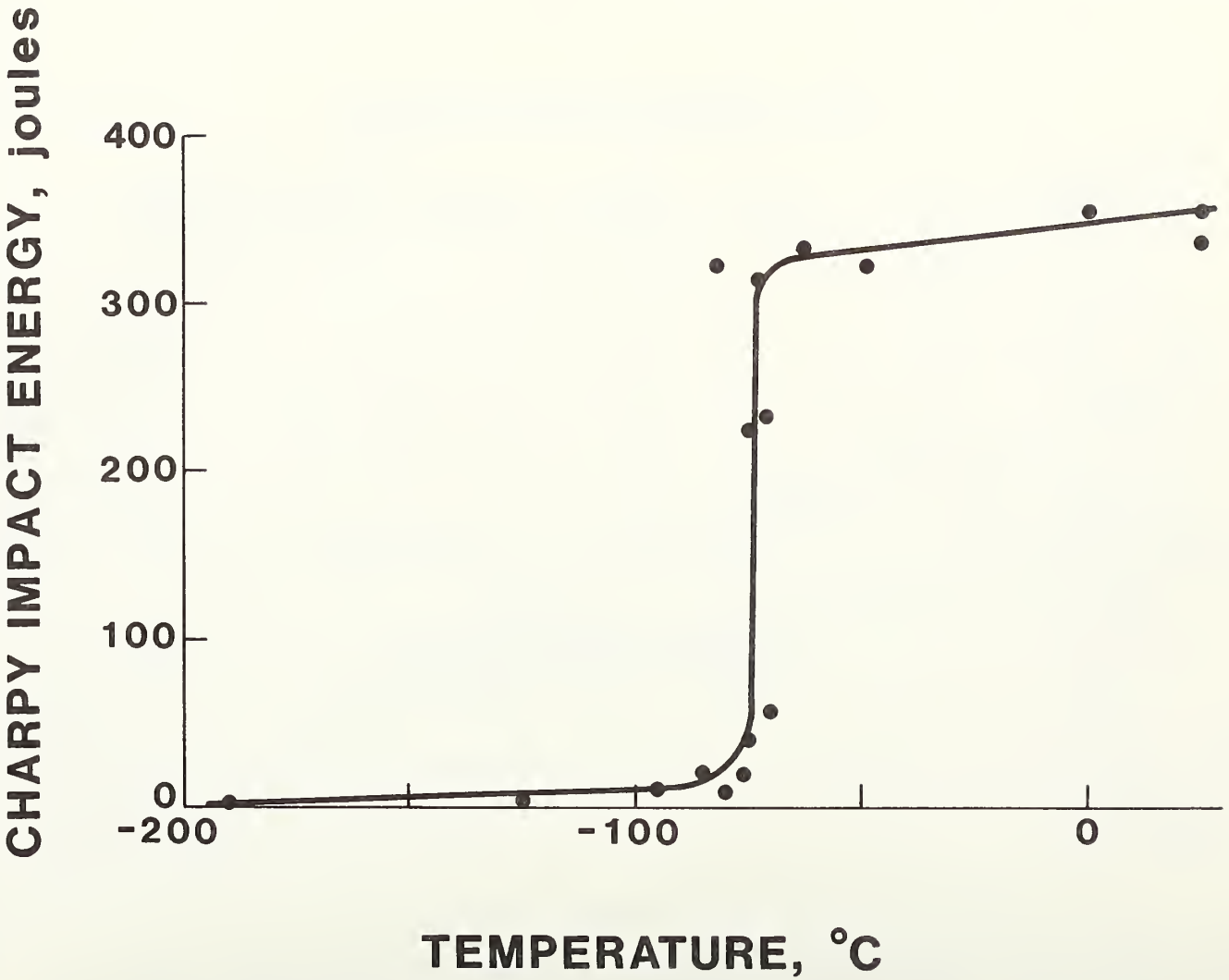

Figure 8. Charpy impact transition curve for ABS grade EH36 steel.

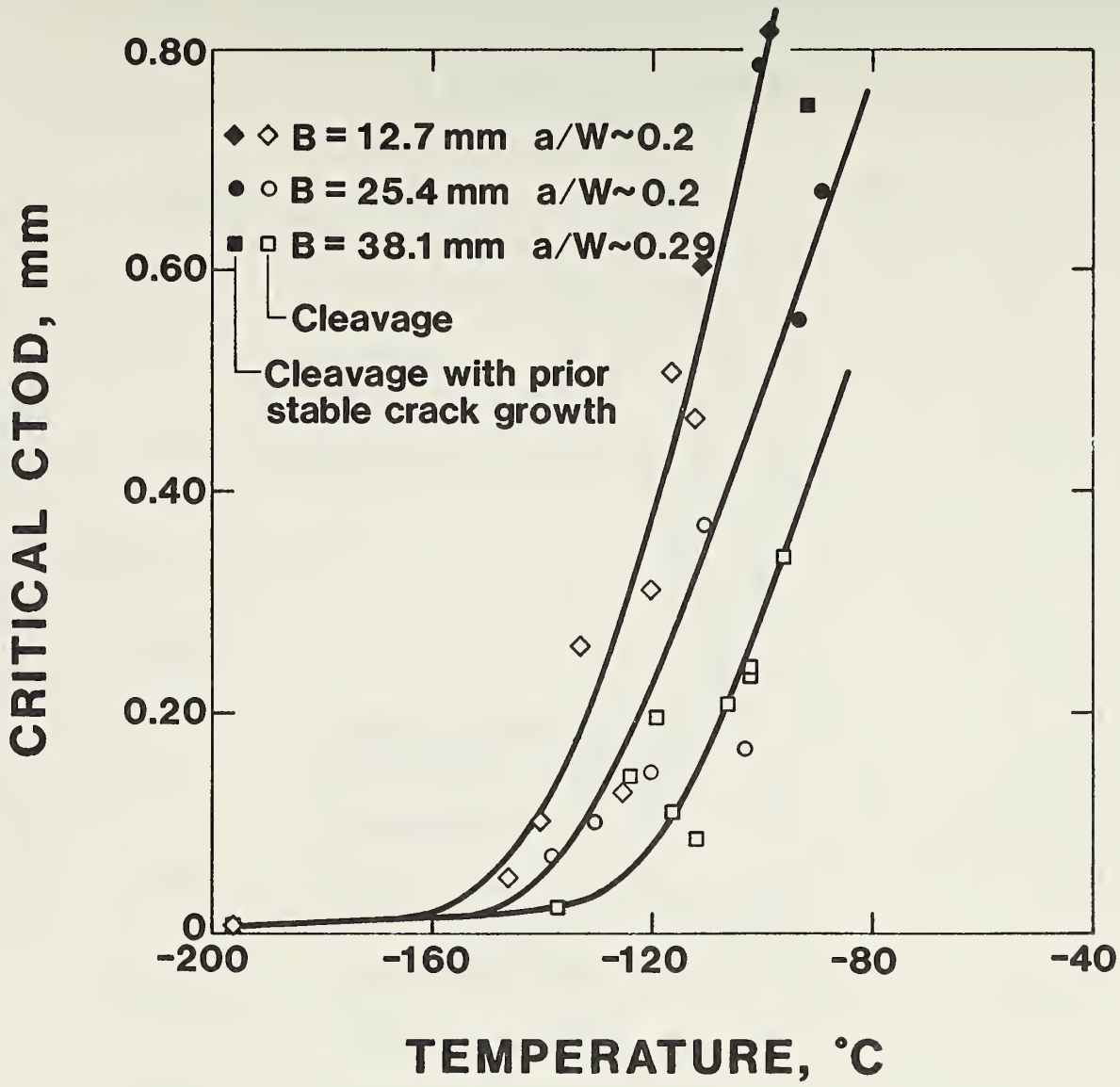

Figure 9. Critical CTOD for cleavage as a function of temperature and specimen thickness for ABS grade EH36 steel. W = 25.4 mm (1.0 in).

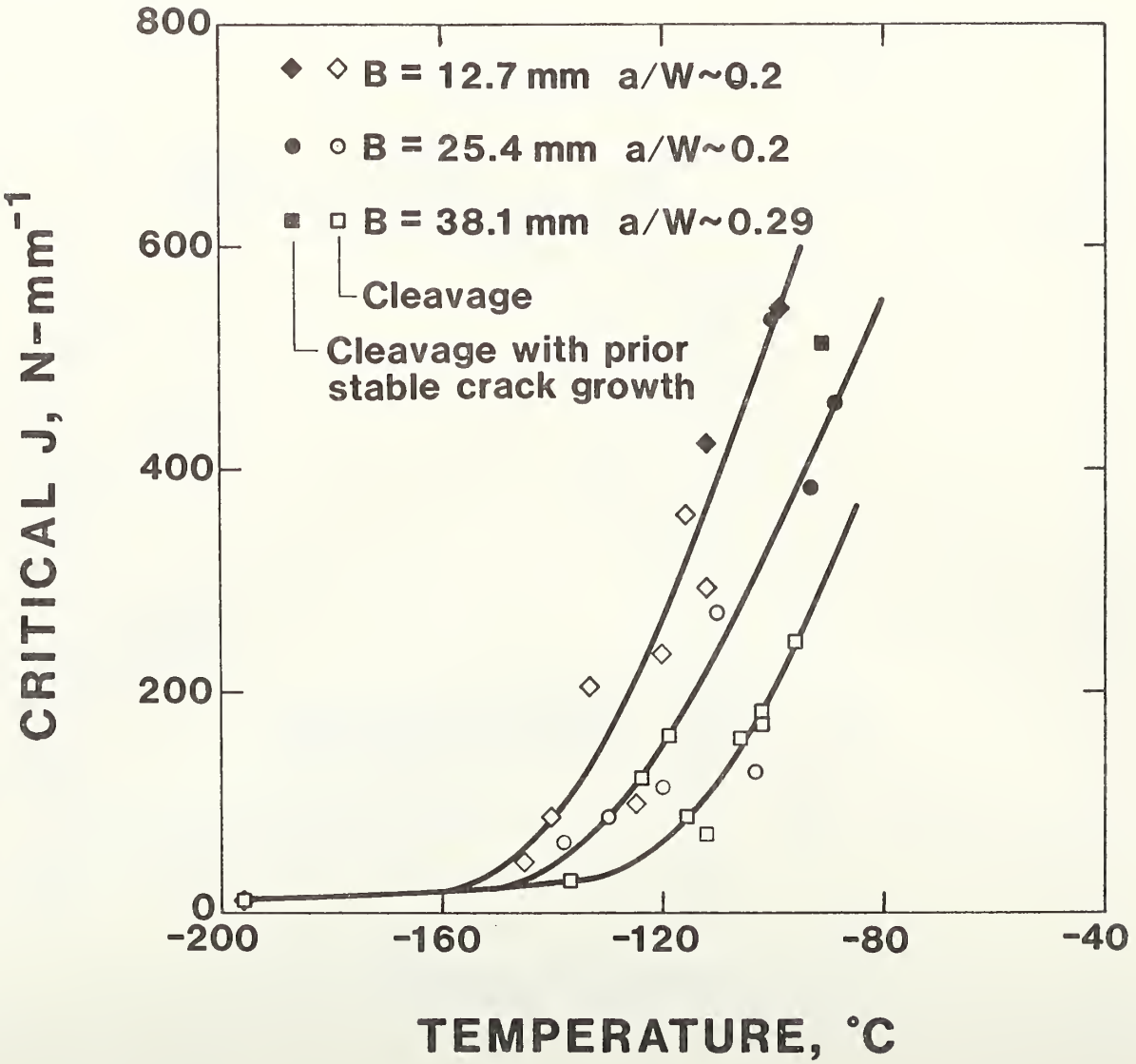

Figure 10. Critical J for cleavage as a function of temperature and specimen thickness for ABS grade EH36 steel. W = 25.4 mm (1.0 in).

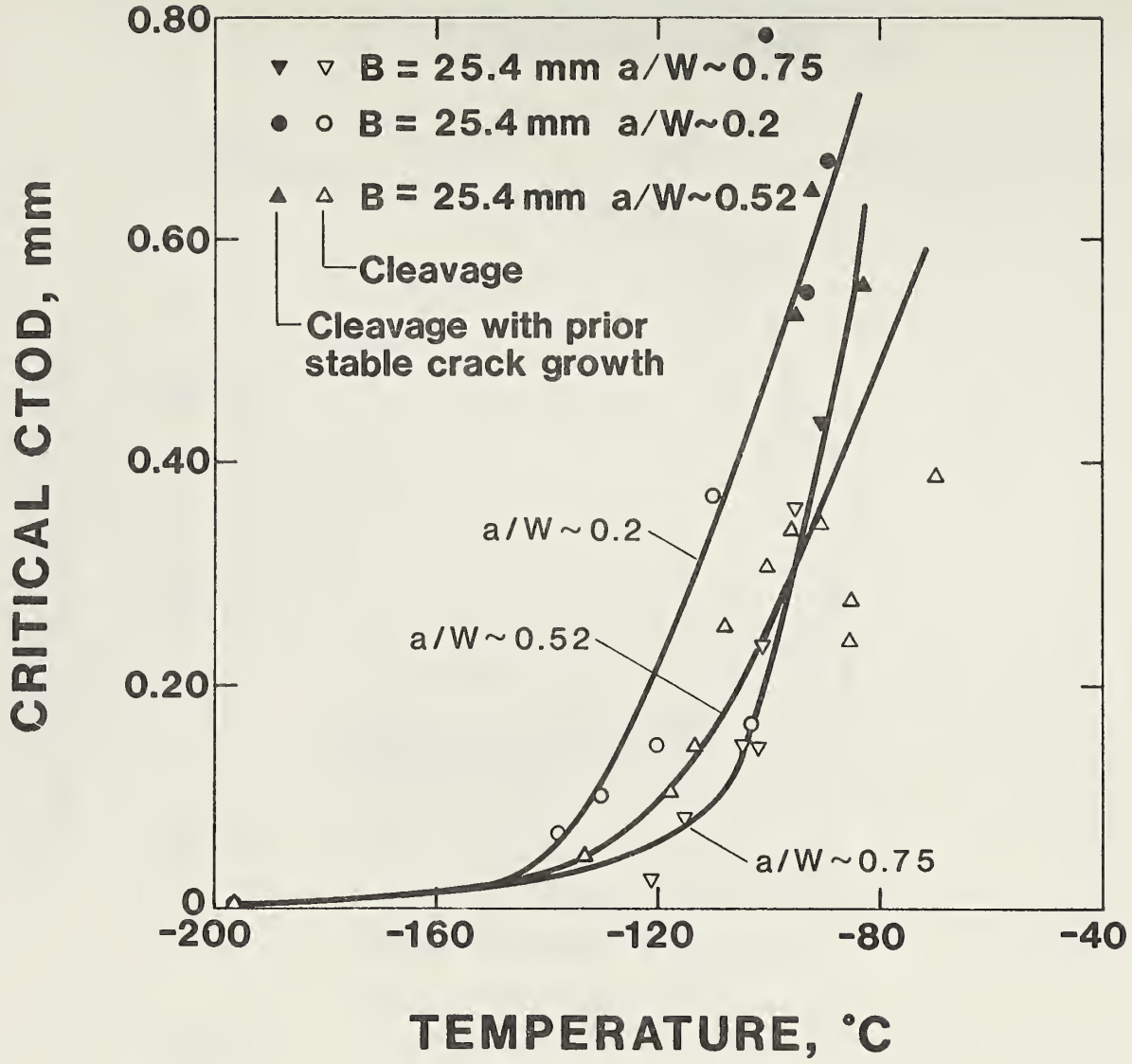

Figure 11. Critical CTOD for cleavage as a function of temperature and crack length for ABS grade EH36 steel. W = 25.4 mm (1.0 in).

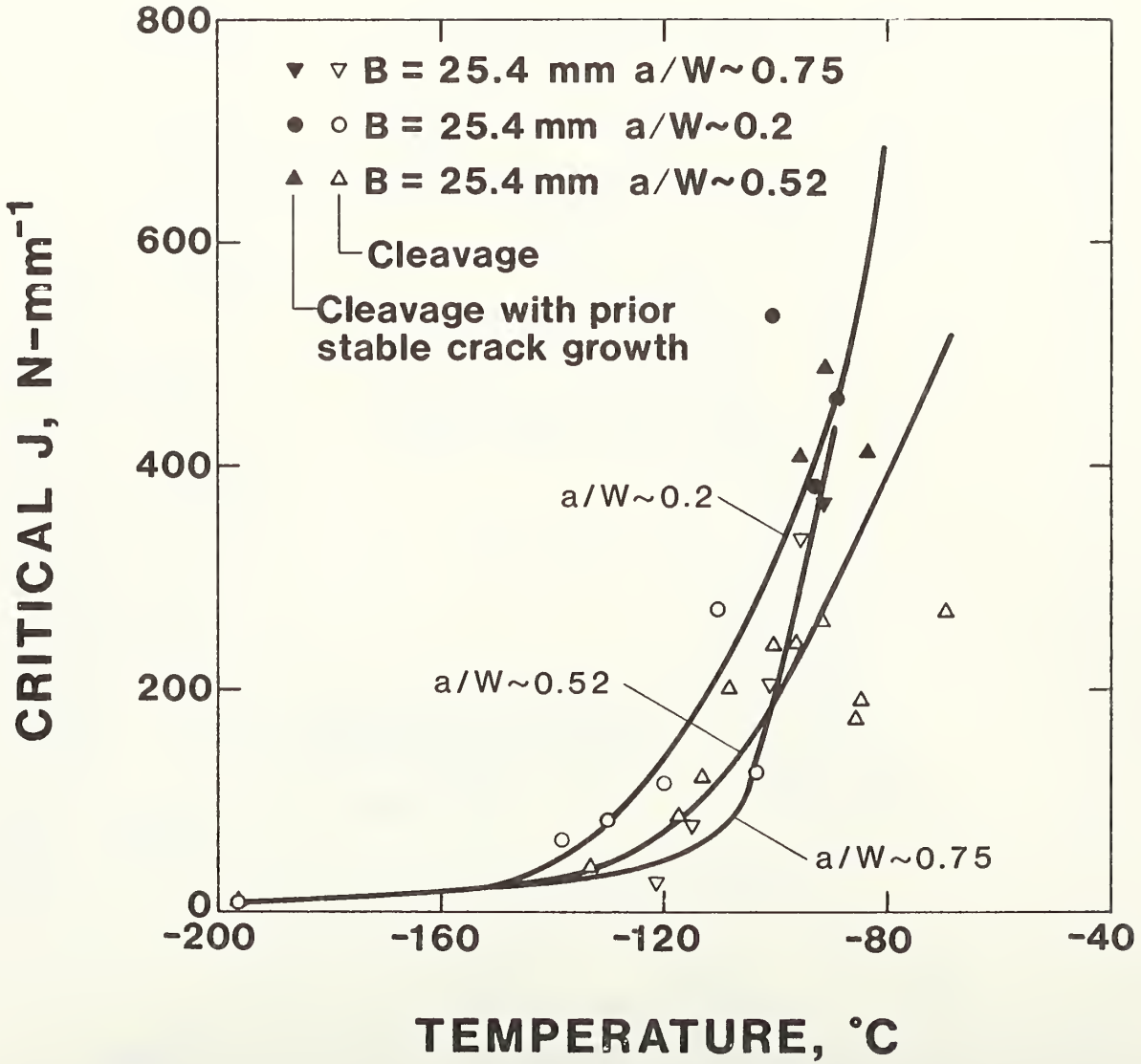

Figure 12. Critical J for cleavage as a function of temperature and crack length for ABS grade EH36 steel. W = 25.4 mm (1.0 in).

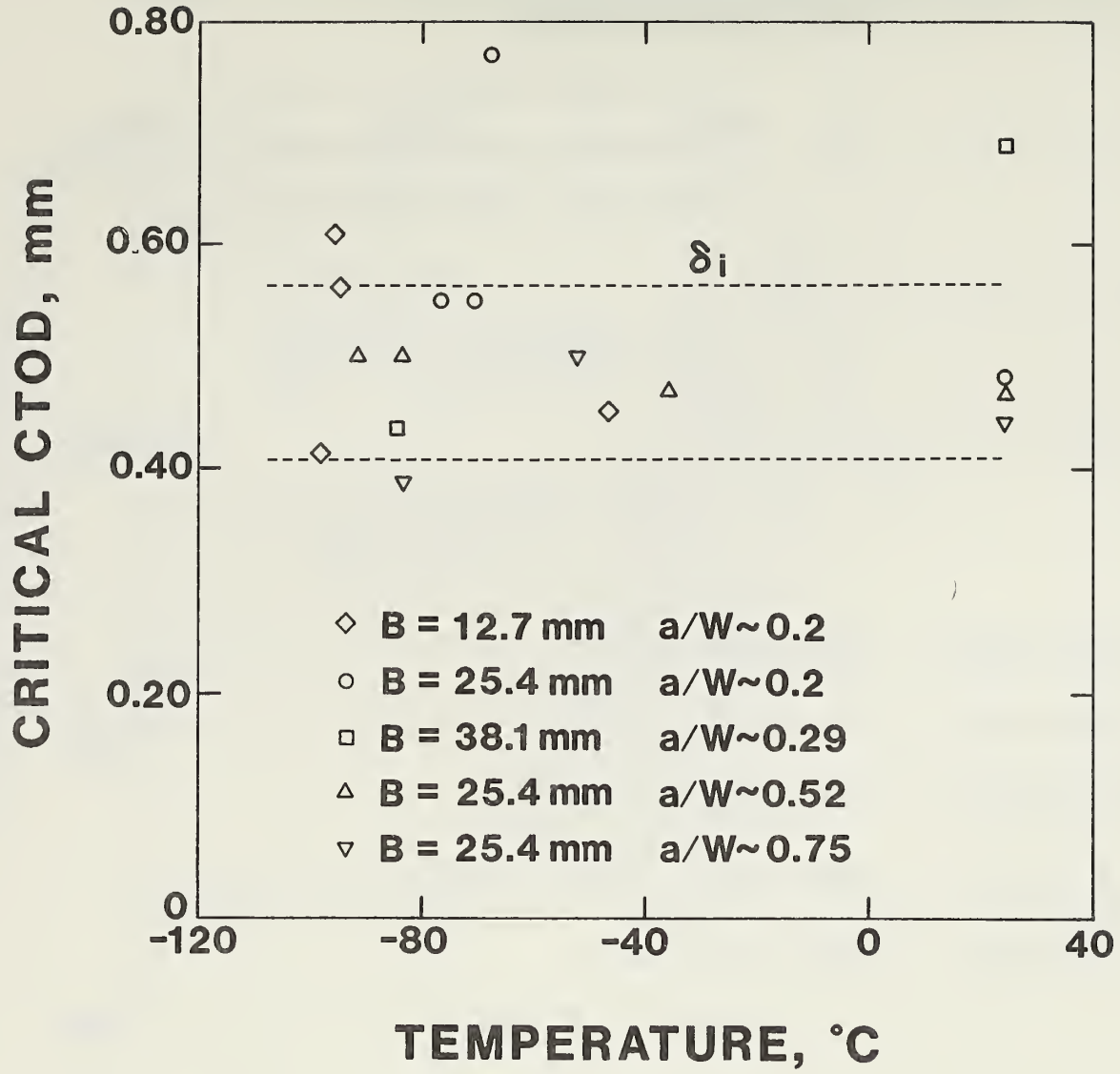

Figure 13. Critical CTOD for the onset of tearing as a function of temperature and specimen geometry for ABS grade EH36 steel. W = 25.4 mm (1.0 in).

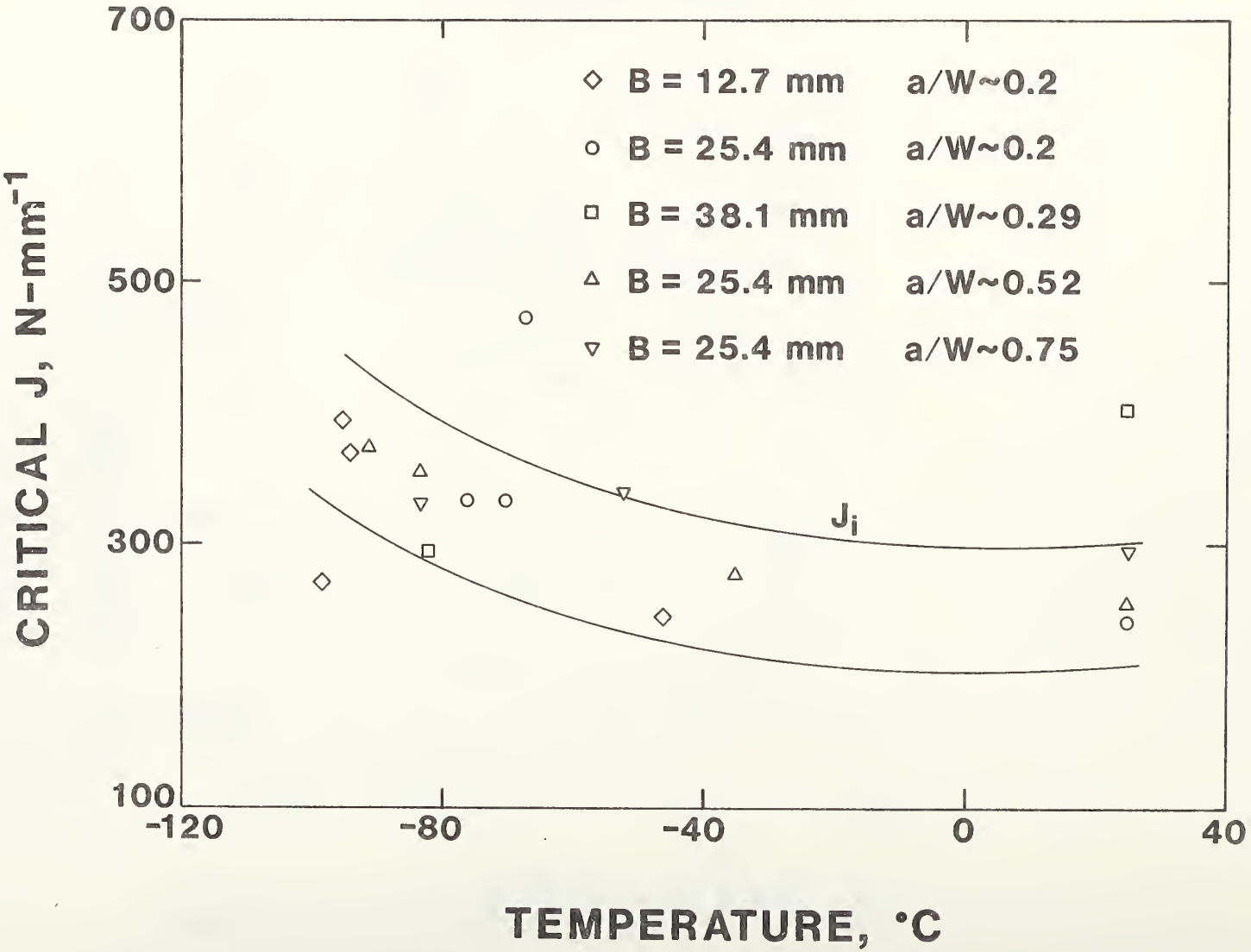

Figure 14. Critical J for the onset of tearing as a function of temperature and specimen geometry for ABS grade EH36 steel. W = 25.4 mm (1.0 in).

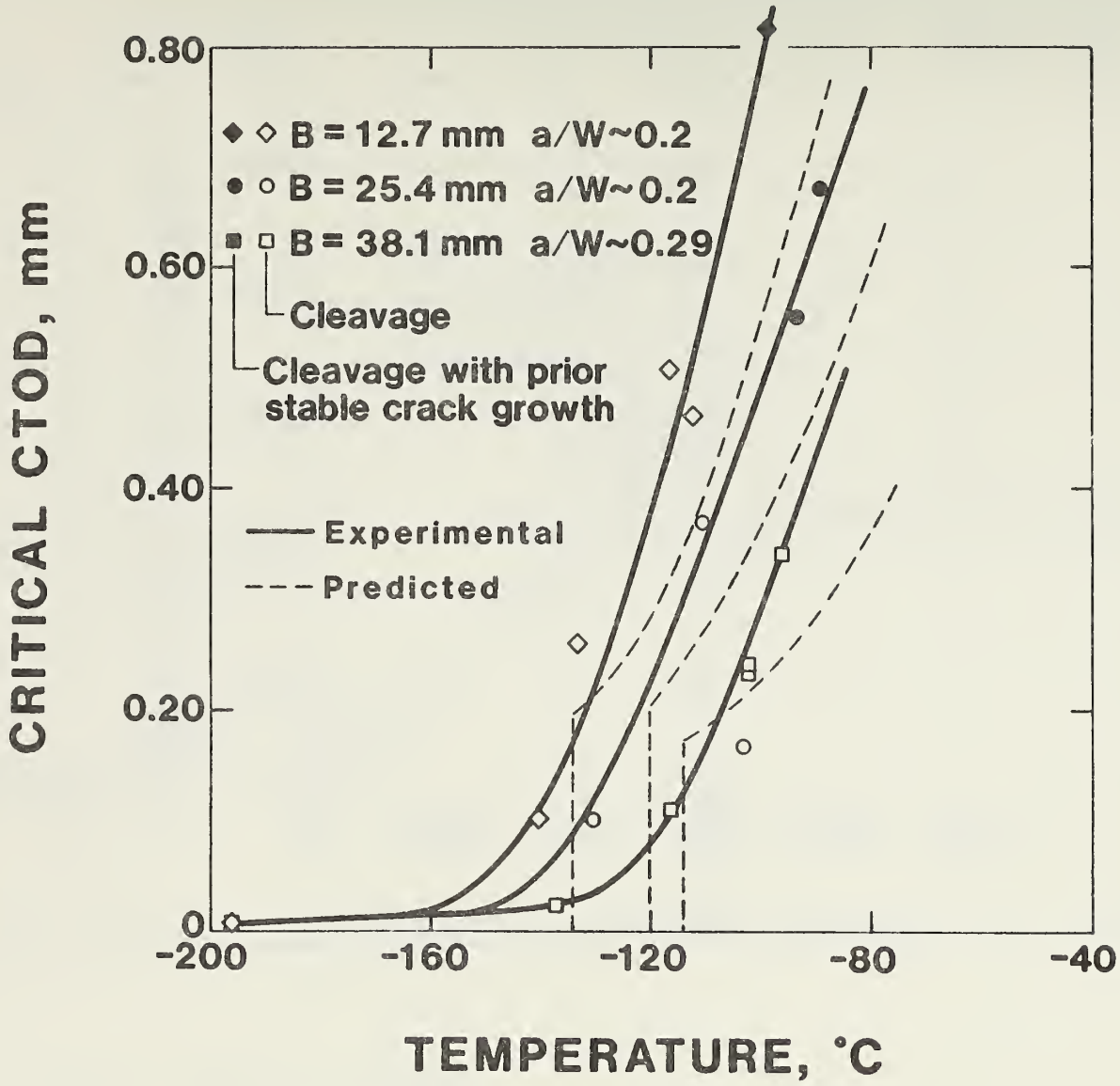

Figure 15. Comparison of predicted and experimental CTOD values as a function of temperature and specimen thickness.

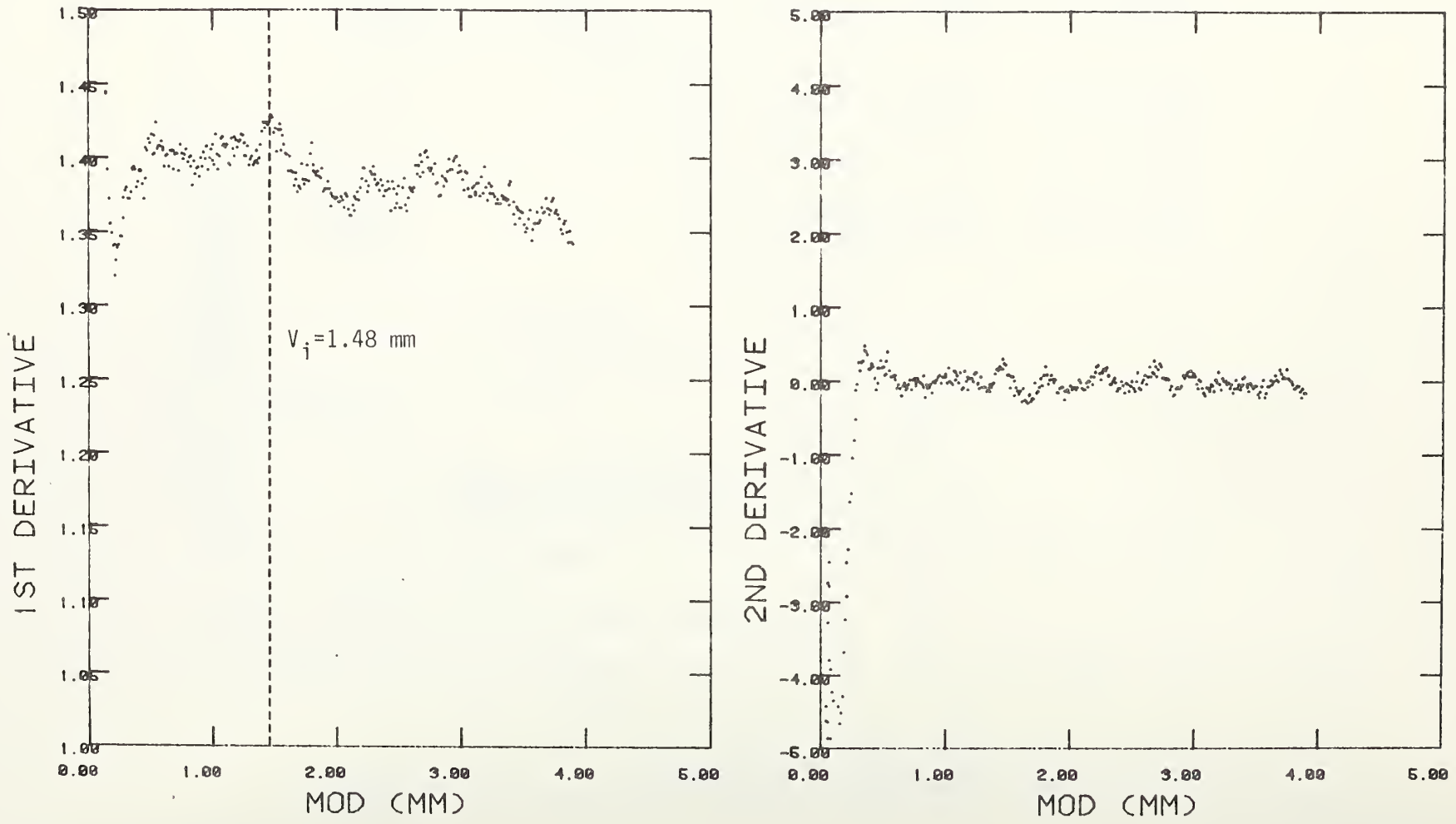

Figure 16. Computer plots of the first and second derivatives of q with respect to V. A sharp drop in the first derivative generally indicates tearing.

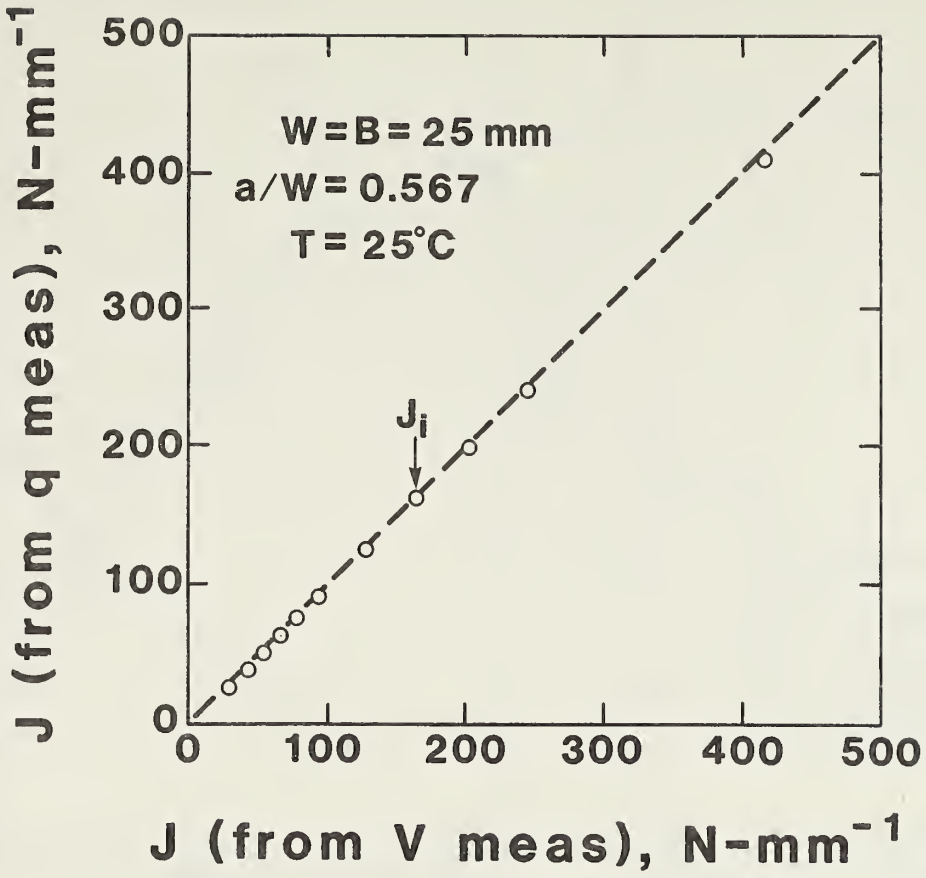

Figure 17. Comparison of J estimates from equations 8 and 9.

SPEC. C-1, 25 C, A/W = 0.2925

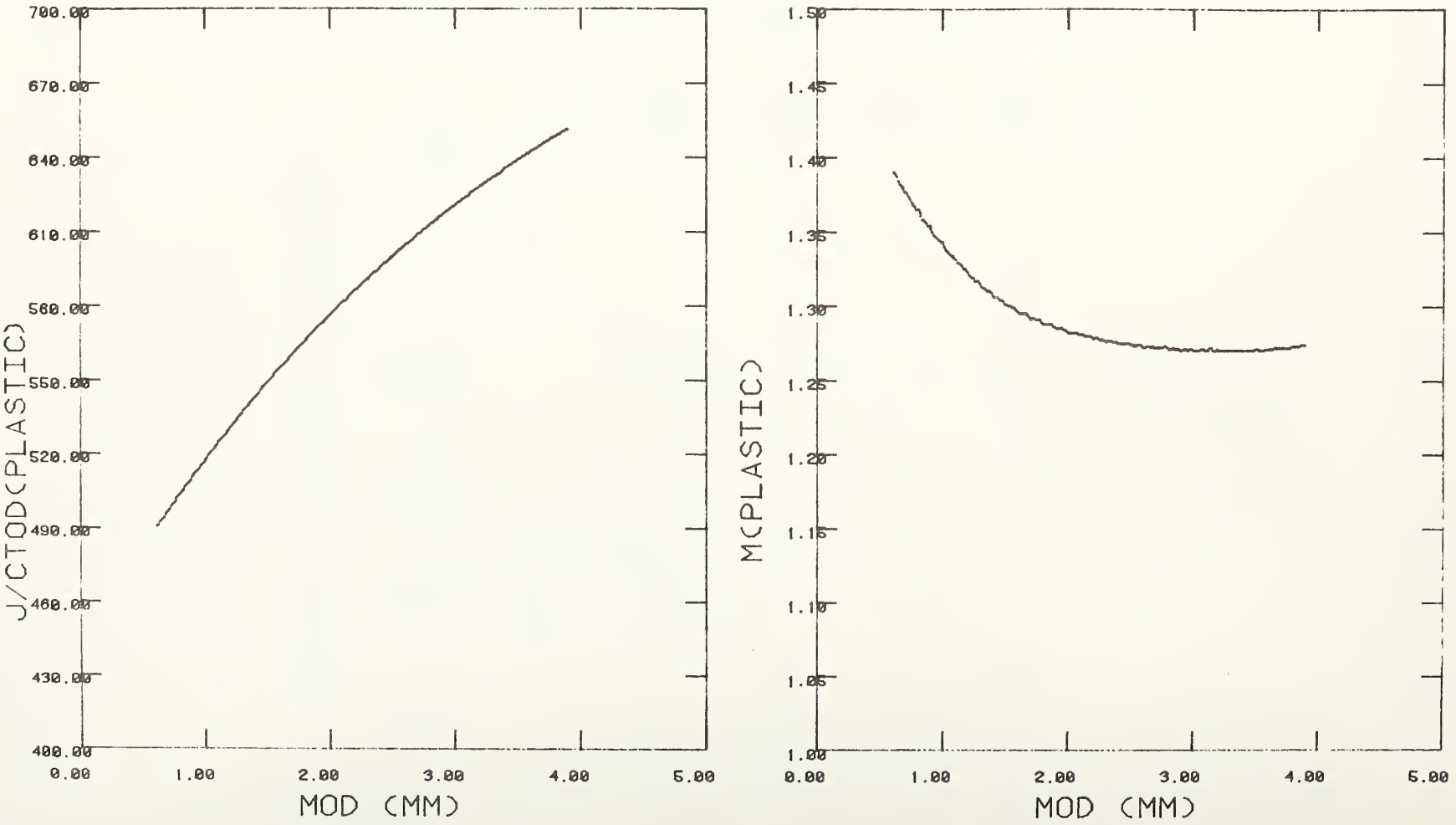

Figure 18. The ratio of the plastic components of J and CTOD and an estimate of the plastic m factor as a function of displacement.

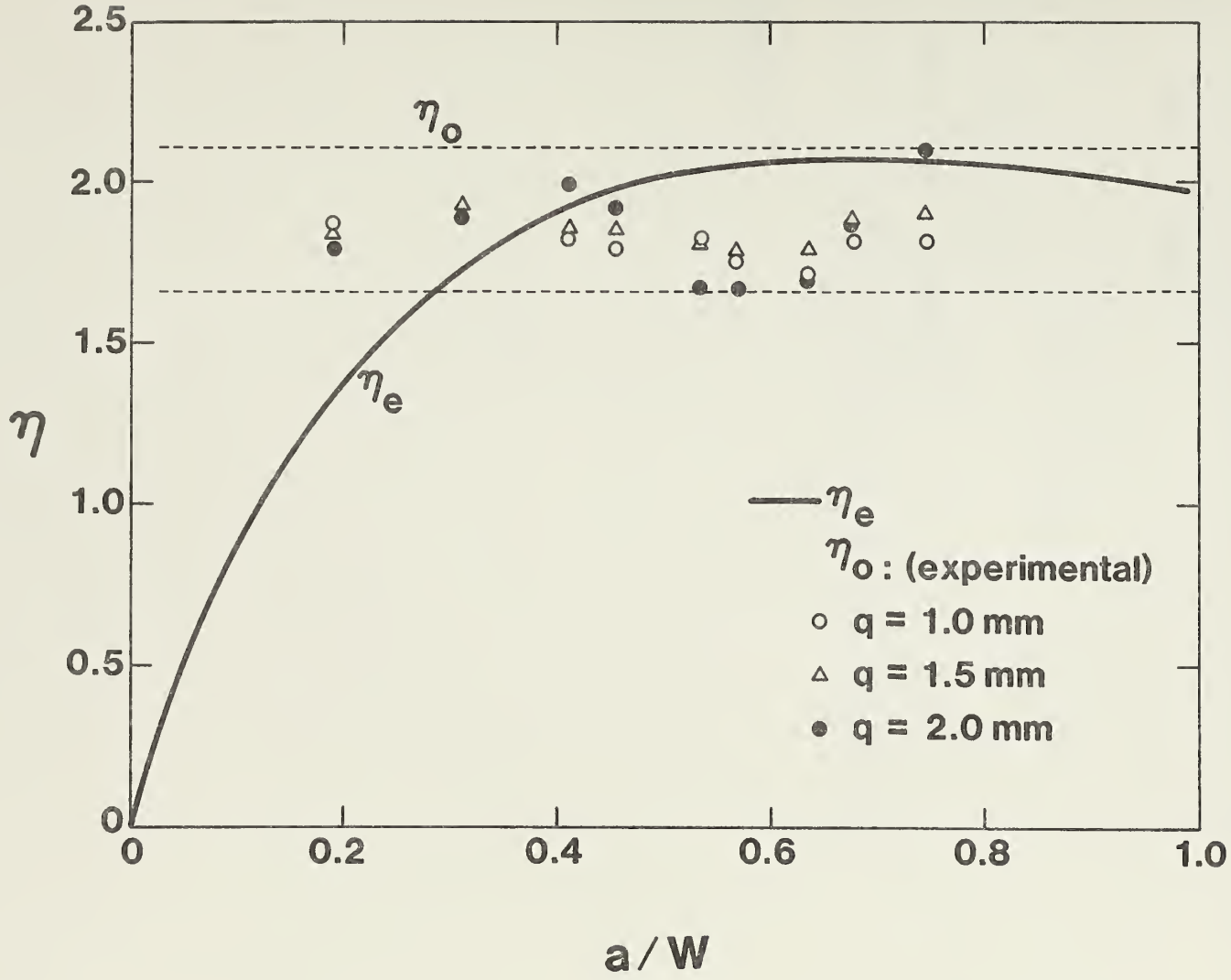

Figure 19. The overall eta factor (η_o) as a function of a/W and displacement. The elastic eta factor curve [17] is superimposed for comparison.

APPENDIX

Literature Review

This literature review covers the basic concepts of fracture mechanics and recent research pertinent to the present study.

CONTENTS

1. LINEAR ELASTIC FRACTURE MECHANICS 53

1.1 The Stress Intensity Factor 53
1.2 Fracture Toughness 54
1.3 Crack Tip Plasticity 55
1.4 Summary Comments 55

2. ELASTIC PLASTIC FRACTURE MECHANICS 56

2.1 The Crack Tip Opening Displacement 56
2.2 J-Integral 58
2.3 Summary Comments 60

3. MICROMECHANISMS OF FRACTURE 61

4. EFFECT OF SPECIMEN SIZE AND CONSTRAINT ON FRACTURE BEHAVIOR 62

5. REFERENCES 64

List of Figures

		Page
Fig. A1.	ASTM E-399 compact specimen for fracture toughness testing.	67
Fig. A2.	Three-point bend specimen used to obtain CTOD test results.	68
Fig. A3.	Notation for critical CTOD values.	69
Fig. A4.	Notation for critical J values.	70
Fig. A5.	The three basic micromechanisms of fracture.	71
Fig. A6.	Schematic representation of possible flow curves for material near the crack tip, illustrating the effect of flow stress on the micromechanism of fracture. (a) Cleavage, (b) cleavage preceded by ductile tearing, and (c) stable crack growth.	12
Fig. A7.	Effect of specimen geometry and plastic zone size on fracture toughness. Specimens must lie to the right of the vertical line to meet ASTM E-399 specifications.	73
Fig. A8.	Effect of constraint on ductile-to-brittle transition behavior.	74
Fig. A9.	Effect of constraint on the micromechanism of fracture. At the temperature represented by the vertical line the low constraint specimen fails by ductile tearing while the high constraint specimen fails by cleavage.	75
Fig. A10.	Effect of specimen thickness on the ductile-to-brittle transition behavior.	76
Fig. A11.	Effect of notch depth on fracture behavior of SENB specimens.	77
Fig. A12.	Effect of type of loading on fracture toughness.	78
Fig. A13.	Attempt to match the crack-tip region constraint (CTRC) of a structure with an SENB specimen.	79

1. LINEAR ELASTIC FRACTURE MECHANICS

The physical basis of fracture mechanics stems from the work of Griffith [1] who demonstrated that the strain energy released upon crack extension is the driving force for fracture. The strain energy, U, is the work done by load, P, causing a displacement, Δ:

$$U = \frac{P\Delta}{2} = \frac{CP^2}{2} \tag{1}$$

where $C = \frac{\Delta}{P}$ = elastic compliance.

The loss of elastic energy upon crack extension of unit area, A, is defined as the strain energy release rate, G:

$$G = -\left.\frac{dU}{dA}\right|_{\Delta} = \frac{P^2}{2}\frac{dC}{dA} = \left.\frac{dU}{dA}\right|_{P}. \tag{2}$$

Irwin and Kies [2] used this relationship to determine the fracture resistance of structural materials, G_c, by measuring the critical load, P_c, in a specimen with a known compliance function, dC/dA.

1.1 The Stress Intensity Factor

Irwin [3], who determined the stress distribution near the tip of a crack located in a linear elastic body, developed a stress analysis basis for fracture mechanics. The magnitude of the crack tip stress field, σ_{ij}, was found to be proportional to a single parameter, K, the stress intensity factor:

$$\sigma_{ij} = \frac{K}{\sqrt{2\pi r}} f_{ij}(\theta) = K \cdot f(\text{position}) \tag{3}$$

where, r and θ are cylindrical position coordinates; r = 0 at the crack tip and θ = 0 in the crack plane. K is a function of the applied stress, σ, crack length, a, and a factor dependent on structural geometry, Y(a):

$$K = Y(a)\sigma\sqrt{a} \tag{4}$$

Tada, Paris and Irwin [4] and Sih [5] have published handbooks of K formulae for various geometries and boundary conditions.

Irwin [3] demonstrated that the strain energy release rate and stress intensity factor are related:

$$K^2 = E'G \tag{5}$$

where, for plane stress, $E' = E$, the elastic modulus; and for plane strain, $E' = E/(1-\nu^2)$, where ν is Poisson's ratio. Thus, it is equivalent to attributing the driving force for fracture to the crack tip stress field, which is proportional to K, or to the elastic strain energy release rate, G. The stress intensity, K, is used more commonly than G because K can be computed for different structural geometries using stress analysis techniques.

1.2 Fracture Toughness

Fracture occurs when the crack tip stress field reaches a critical magnitude, i.e., when K reaches K_c, the fracture toughness of the material. K_c is a mechanical property that is a function of temperature, loading rate and microstructure, much the same as yield strength is; however, K_c is also a function of the extent of crack tip plasticity relative to the other specimen (or structural) dimensions. If the plasticity is small compared to the specimen dimensions and the crack size, then K_c approaches a constant minimum value defined as K_{Ic}, the plane strain fracture toughness.

Measurements of fracture toughness based on linear elastic theory are limited to the case of plane strain testing in accordance with ASTM E-399 [6].

$$B,\ a,\ W\text{-}a \geq 2.5\ \left(\frac{K_{Ic}}{\sigma_{ys}}\right)^2 \tag{6}$$

where B, a, and W are defined in Fig. A1. The specimens are precracked by fatigue
cycling to an initial crack length of a/W = 0.5 and subsequently loaded to failure. K_{Ic} is calculated from the critical load, P_Q, the measured crack length, the specimen dimensions and the specimen calibration function, $Y(\frac{a}{W})$, as follows:

$$K_Q = \frac{P_Q}{B\sqrt{W}}\ Y\left(\frac{a}{W}\right). \tag{7}$$

$K_{Ic} = K_Q$ if all the conditions of ASTM E399 are met, i.e., precracking procedures, load-displacement record, specimen dimensions, etc.

1.3 Crack Tip Plasticity

Applicability of the linear elastic analysis has been extended to conditions approaching net section yielding by correcting for the zone of plasticity that exists at the crack tip [7]. The idea is that the plastic material at the crack tip strains without carrying the incremental load; therefore, in the elastic sense, the crack behaves as if it were slightly longer. The adjustment is made by adding the radius of the plastic zone, r_y, to the apparent crack length:

$$K = Y(a+r_y)\ \sigma\sqrt{a+r_y} \tag{8}$$

$$r_y = \frac{1}{2\pi}\left(\frac{K}{\sigma_Y}\right)^2 \tag{9}$$

where, σ_Y is the yield strength at the crack tip. The r_y correction modifies the crack tip stress field to account for the elastic stress redistribution due to the localized plasticity.

The extent of crack tip plasticity is influenced by specimen dimensions. This is particularly true for thickness. As specimen thickness increases, σ_Y increases from σ_{ys} to $\sqrt{3}\ \sigma_{ys}$ due to through-the-thickness elastic constraint [8]. The maximum value of σ_y is reached when the plastic zone size is limited to about 5% of the thickness. Thus, in a given material, the plastic zone size as computed by Eq. (9) can vary with thickness by a factor of three -- leading to a strong dependence of K_c on thickness.

1.4 Summary Comments

The crack tip stress field is the driving force for fracture and the magnitude of this stress field is proportional to the stress intensity factor, K. K is a function of crack size, applied stress and structural geometry and can be computed using stress analysis methods. The resistance to fracture is a material property defined as the fracture toughness, K_c; fracture occurs when $K = K_c$. Thus, for a given structural geometry and material, critical crack sizes can be determined as a function of applied stress and vice-versa:

$$a_c = \left[\frac{K_c}{\sigma Y(a)}\right]^2 . \qquad (10)$$

The approach is applicable to conditions of localized crack tip plasticity, i.e., where $\sigma \leq .8\sigma_{ys}$ or $r_y \leq 0.3a$, when the r_y correction is used to account for crack tip plasticity [9].

2. ELASTIC-PLASTIC FRACTURE MECHANICS

Many of the high toughness structural materials used for arctic structures undergo extensive plastic deformation prior to fracture. Thus, the concepts of linear elastic fracture mechanics must be extended to account for elastic-plastic behavior. The two approaches of interest in the present investigation are the crack tip opening displacement (CTOD) and the J integral.

2.1 The Crack Tip Opening Displacement

The CTOD concept is a crack tip strain criterion for fracture stemming primarily from the work of Wells [10,11]. Wells' hypothesis was that the opening of the crack faces was strictly related to the crack extension force, G, and the stress intensity factor, K, under locally plastic conditions. Wells used an energy balance argument to derive an expression for CTOD [11]:

$$\delta = \frac{K_I^2}{E\sigma_y} \quad \frac{G_I}{\sigma_y} \qquad (11)$$

where δ is the CTOD.

In 1965 Burdekin and Stone [12] illustrated how the CTOD concept could be used to extend the capability of conventional fracture mechanics to the elastic-plastic case. A Dugdale strip-yield model [13] was used to develop the following equation for plane stress Mode I crack-tip displacements under monotonic loading.

$$\delta = \frac{\sigma a}{\pi E} \ln \sec \left(\frac{\pi}{2} \frac{\sigma}{\sigma_y}\right) \qquad (12)$$

A fracture toughness test method based on the CTOD concept was developed by investigations at the Welding Institute [14-16]. The CTOD test specimen contained a fatigue-precracked notch and was loaded in three-point bending to

fracture. The critical CTOD was obtained from the load versus clip-gage displacement record. The clip-gage displacement, V_g, was measured across the notch mouth as shown in Fig. A2. The V_g was converted to CTOD using the following relationship [14].

$$\delta = \frac{V_g}{1 + \left(\frac{a+z}{r(W-a)}\right)} \tag{13}$$

where z = knife edge thickness
a = crack length
W = specimen width
r = rotational factor

This equation was derived assuming that the crack faces opened by a simple hinge mechanism about a center of rotation. The value of r was assumed to be 0.5 in early work.

The current British standard for CTOD testing [17] specifies that the CTOD be calculated from the following relationship.

$$\delta = \frac{K^2}{2\sigma_y E'} + \frac{0.4(W-a)V_p}{0.4W + 0.6a + z} \tag{14}$$

where the first term is the elastic component of CTOD, δ_e, and the second term is the plastic component, δ_p. The plastic component of the clip-gage displacement, V_p, is estimated by constructing a line, parallel to the elastic-loading line, from the critical point on the load-displacement curve to zero load. The elastic component of the clip gage displacement is then subtracted from the total displacement. The stress intensity factor for the elastic CTOD calculation is obtained from the following relationship.

$$K = \frac{YP}{BW^{1/2}} \tag{15}$$

where P is the applied load and Y is the stress intensity coefficient. Y is a function of specimen geometry and can be obtained for a given crack length to width ratio (a/W) from the test standard [17].

A more detailed description of the CTOD test method is given in the body of this report. The type of critical CTOD reported depends on the nature of the observed fracture event. This is illustrated schematically in Fig. A3 for a steel which undergoes a ductile-to-brittle transition. At low temperatures the steel fails by cleavage and δ_c is measured experimentally. As the test temperature increases cleavage becomes less favorable and the fracture toughness increases. Eventually the fracture mode changes to microvoid coalescence and the crack grows in a stable manner. δ_i is defined as the value of CTOD at the onset of tearing. At temperatures slightly above the fracture mode change, stable tearing can be followed by unstable cleavage. When this occurs, δ_u is measured at the instability point. On the upper shelf of toughness, the steel reaches a point of plastic collapse when the work-hardening cannot keep pace with the decrease in ligament area caused by stable crack growth. δ_m is then measured at the point of maximum load in a bend test. δ_R is the total CTOD, i.e. δ_i plus the portion of CTOD associated with tearing. A plot of δ_R versus Δa, is the resistance (R) curve, , a measure of a material's resistance to crack growth. Figure A3 also shows that δ_i is not a strong function of temperature, but it is a function of the inclusion content.

2.2 J-Integral

The J-integral is a characterization developed by Rice [18] of the elastic-plastic field in the vicinity of the crack tip. The use of the J-integral as a fracture criterion was suggested and experimentally demonstrated by Begley and Landes [19]. J is defined as the line integral:

$$J = \int_\Gamma \left[w dy - \vec{T} \left(\frac{\partial \vec{u}}{\partial x} \right) ds \right] \qquad (16)$$

where, Γ is any contour surrounding the crack tip,

w is the strain-energy density,

$\vec{T}$ is the stress vector normal to Γ,

$\vec{u}$ is the displacement vector, and

s is the arc length along Γ.

The J-integral is path independent for linear and non-linear elastic materials [18] and nearly so for most structural materials under monotonic loading conditions [20]. Thus, J can be computed using numerical methods by analyzing

along a contour away from the crack tip, i.e., in a region where the analysis methods are quite accurate. This relieves the uncertainties of the crack tip region -- a problem that seriously limits the usefulness of the CTOD method.

An equivalent interpretation is that J is equal to the change of potential energy U, upon an increment of crack extension of unit area, A:

$$J = - \frac{dU}{dA}. \tag{17}$$

For the linear elastic case the potential energy equals the strain energy and, therefore, Eq. (17) is the same as Eq. (2) and J = G. Thus, J appears to be a logical extension of linear elastic fracture mechanics into the elastic-plastic range. Due to the irreversibility of plastic deformation, the energy interpretation of the J-integral does not apply to the process of crack extension in elastic-plastic materials -- as G is for elastic materials. J is simply an analytically convenient, measurable parameter that is a characteristic of the elastic-plastic field at the crack tip. The contribution of Begley and Landes [19] was to demonstrate that crack initiation under elastic-plastic conditions occurs at a characteristic value of J, called J_{Ic}, that is related to K_{Ic} in the same way G is related to K in Eq. (5). Thus, J integral methods can be used to determine K_{Ic} in specimens significantly smaller than the size requirements of Eq. (6).

Methods of measuring J_{Ic} are covered by ASTM standard E-813. A deeply notched specimen of the compact tension or single-edge-notch-bend design is precracked to $a/W \cong 0.6$. The specimen is loaded incrementally to a series of J-levels. After each increment of loading, J and the crack extension, Δa, are measured. The load-displacement curve is recorded on an X-Y plotter. Displacement is measured along the load line. J is calculated from the load-displacement record and specimen dimensions using:

$$J = \frac{\eta A}{bB}, \tag{18}$$

where A is the area under the load displacement record, b is the ligament (W-a), and η is a dimensionless parameter dependent on specimen geometry. Δa is measured by either the crack marking technique or the unloading compliance technique described in ASTM E-813. The results of a test series are plotted

as J versus Δa, and the J_{Ic} is defined as the extrapolation of the best-fit curve to the blunting line defined by $J = 2\sigma_Y \Delta a$. K_{Ic} is related to J_{Ic} as follows:

$$K_{Ic}(J) = \sqrt{E' J_{Ic}} \tag{19}$$

A more detailed description of the J-integral test method is given in the body of this report.

The J_{Ic} test method is limited to measurement of the onset of ductile tearing. Thus, it is not applicable to the measurement of fracture toughness when cleavage is the micromode of fracture. Recently Dawes [26] has proposed the adoption of a critical J notation equivalent to the CTOD notation of Fig. A3. This notation, shown in Fig. A4, would make the J concept applicable to all micromechanisms of fracture. This proposed notation is used in the present study.

2.3 Summary Comments

The CTOD and J-integral concepts are efforts to define single parameter characterizations of the fracture process that are applicable to linear elastic and general yielding fracture. In the CTOD concept, attention is focused at the crack tip; fracture theoretically occurs when a critical displacement develops at the crack tip. The J-integral concept examines the stress-strain conditions along an arbitrary contour away from the crack tip; fracture theoretically occurs when the potential energy available for crack extension reaches a critical value defined by J. For the linear elastic case, δ_c and J_{Ic} are consistent with the linear elastic fracture criteria:

$$G_{Ic} = \frac{K_{Ic}^2}{E'} = J_{Ic} = \sigma_Y \delta_c. \tag{20}$$

There has been a great deal of research in recent years on ductile fracture. Models have been developed to predict fracture by tearing instability using J-integral R-curves and to predict fracture by plastic collapse using limit load expressions [21]. This work is not reviewed here because it is not directly relevant to fracture of structural steels at low temperatures.

3. MICROMECHANISMS OF FRACTURE

Fracture usually occurs by one of three mechanisms: ductile tearing, brittle cleavage, or intergranular cracking. The three mechanisms, shown schematically in Fig. A5, are competitive. That is, the fracture mode will depend on which condition is reached first: the critical strain for ductile tearing, the critical stress for cleavage, or the stress that exceeds the cohesive strength of the grain boundary. The conditions for ductile tearing and brittle cleavage are represented in Fig. A6. Note that fracture may initiate by ductile tearing and, as the stress increases, convert to cleavage. Fracture toughness is strongly influenced by the micromode of fracture, and thus it is important in a study of the ductile-to-brittle transition to identify the governing fracture mode.

To be suitable for OCS platforms, structural alloys should fracture in a ductile manner at the minimum service temperature. Ductile tearing, also called microvoid coalescence, is caused by the formation and growth of the voids that eventually comprise the fracture surface. Thus, the toughness of ductile metals is related to the factors that influence the nucleation and growth of voids. Voids nucleate most readily at second-phase particles, such as inclusions and precipitates (1 to 10 μm in size), as a result of interfacial separation, fracture of the particle, or matrix separation caused by strain concentration near the particle. Voids grow and coalesce by ductile tearing of the matrix. Ductile tearing resistance is a function of the strength and ductility of the matrix. As matrix strength increases, less energy is dissipated by plastic deformation during tearing and toughness is reduced. Increased matrix strength also tends to activate additional void nucleation sites. Consequently, there is usually an inverse relationship between fracture toughness and yield strength when the fracture mode is ductile tearing.

Brittle fracture requires less energy for surface formation than ductile fracture. Lower energy fracture modes include cleavage and intercrystalline (grain boundary) fracture. Cleavage is a fracture mode in which material separation proceeds along preferred crystallographic planes without sizable plastic deformation prior to fracture. Metals subject to cleavage, such as structural steels, usually have a large increase in yield strength as temperature is decreased. Cleavage occurs when the cleavage fracture stress is reached before the strain required for void formation is exceeded. Intercrystalline fracture occurs when the cohesive strength of the grain boundary is

exceeded before cleavage or ductile fracture occurs. As matrix strength increases with decreasing temperature, intergranular failure may occur more readily in a susceptible alloy. However, as a class, the structural steels that are candidates for arctic construction are not susceptible to intergranular fracture.

4. EFFECT OF SPECIMEN SIZE AND CONSTRAINT ON FRACTURE BEHAVIOR

Specimen geometry can have a substantial effect on fracture toughness as illustrated in Fig. A7. As thickness, crack length, and uncracked ligament length become large compared to the plastic zone the fracture toughness reaches a minimum value defined by K_{Ic}. The ASTM E-399 standard is designed to measure this lower bound fracture toughness. The behavior in Fig. A7 is due to the fact that large specimens promote a maximum degree of triaxiality at the crack tip, thereby increasing the yield stress. This increase in yield stress tends to promote fracture since it is easier to reach the fracture stress. Smaller, less constrained specimens tend to lose triaxiality so that a greater amount of plastic deformation must occur before the fracture stress can be reached in the plastic zone.

The amount of constraint in the region of the crack tip will depend on the yield strength of the material and the geometry of the fracture specimen. The specimen geometry consequently has an effect on the ductile-to-brittle transition behavior of steels. This is illustrated schematically in Fig. A8. The lower-bound LEFM curve is shown along with four hypothetical specimen geometries with varying degrees of constraint. The lowest constraint geometry, represented by the curve farthest to the left, has the lowest transition temperature and has the highest toughness at a constant temperature. The vertical line in Fig. A8, drawn at an arbitrary temperature in the transition region reveals that a wide range of toughness values could be obtained for a material at a given test temperature, depending on the constraint of the fracture specimen.

Figure A9 shows how varying degrees of constraint can lead to different micromodes of fracture at a constant temperature. This represents a potentially dangerous situation when using fracture toughness data from small specimens to design large structures. At temperatures where ductile tearing is the micromode of fracture, it is permissible to predict the fracture toughness of large structures from small specimen data because J_i and δ_i are

not a strong function of geometry [22,23]. However, at temperatures where cleavage may be the micromode of fracture, a crack in a small fracture specimen may grow in a stable and ductile manner while a large structure could fail catastrophically by cleavage and have much lower toughness than predicted in the small scale test.

There is a very limited amount of data in the literature which shows the effect of specimen geometry on fracture toughness. An added handicap is that many of the authors do not specify the micromode(s) of fracture which they observe. Since it is impossible at this time to describe quantitatively the effect of specimen size on constraint the following section will offer a purely qualitative description based on theory and a limited amount of experimental data.

A number of investigators [23-28] have studied the effect of specimen thickness on the fracture toughness of various materials. Figure A10 illustrates the effect of thickness on the ductile-to-brittle curves of ferritic steels. Note that an increase in thickness from B to 2B has a greater effect than increasing thickness from 2B to 3B. This is because increases in thickness increase constraint at a decreasing rate until a saturation thickness (plane strain) is reached.

It should be noted that not all investigators attribute the decrease in toughness with specimen size to constraint. Although the average toughness of the smaller size specimens is higher than the K_{Ic} value, the lowest toughness values for the smaller specimens can be lower than the large specimen K_{Ic} value. This scatter phenomena can be explained by the statistical effect of inhomogeneity along the crack front [29]. This inhomogeneity will cause greater scatter in small specimen results because the volume of material sampled is less. Landes and Begley [29] maintain that this statistical effect alone is sufficient to explain the size effect on fracture toughness. They applied a Weibull [30] statistical distribution to predict K_{Ic} from scattered small specimen results. However, Lin [31] believes that this approach gives a too conservative estimate of K_{Ic}. Lin points out that the model of Landes and Begley based on the Weibull distribution erroneously predicts that K_{Ic} approaches zero as the size of samples approaches infinity. Also, Lin used

the Ritchie-Knott-Rice model for cleavage fracture [32] to show that fracture toughness increases from plane strain to plane stress conditions.

It is likely that the size effect on fracture toughness is caused both by constraint and statistical effects. It is difficult, however, to separate out the statistical effects in order to quantitatively study constraint. The experimental scatter in the ductile-to-brittle transition region is often so great that it masks the constraint effects.

The relative crack length and ligament length can also affect crack tip constraint. Figures A7 and A11 show schematically the consensus results of a number of investigations [22-28, 33-35] of the effect of crack length to width ratio. At a constant temperature the fracture toughness is relatively high for short cracks but decreases rapidly with crack length until a lower plateau is reached (Fig. A7). For very deep cracks ($a/W > .75$) the toughness increases rapidly with crack length. This phenomena can be explained as follows [36]. When the crack tip is near the center of the specimen the constraint is maximized because a maximum amount of material surrounds the crack tip. When the crack tip is near a free surface, as in a very deep or shallow crack, the constraint can be relaxed by plastic deformation at the free surface.

In addition to specimen geometry, the type of loading can affect crack-tip constraint. Bending produces more constraint than tensile loading because of the compressive stress below the neutral axis of a bend specimen. The corresponding effect of loading type on the fracture behavior of steels is illustrated in Fig. A12. The Welding Institute in Great Britan utilizes this effect when assessing the fitness for service of structures containing cracks [36]. Figure A13 shows a structure with a hypothetical defect along with the corresponding SENB specimen. The Welding Institute uses a square-section specimen with the depth, W, matching the plate thickness and the crack length, a, matching that of the structure. It is then assumed that the increased constraint in the SENB specimen due to bending will offset the loss of constraint due to the lack of plane strain in the test specimen. This assumption has not been satisfactorily verified.

5. REFERENCES

[1] A. A. Griffith, Phil. Trans. Roy. Soc. 221A, 1920, p. 163.

[2] G. R. Irwin and J. A. Kies, Welding J., 33, 1954, p. 193s.

[3] G. R. Irwin, Trans. ASTM, J. Appl. Mech., 24, 1957, p. 361.

[4] H. Tada, P. C. Paris, and G. R. Irwin, The Stress Analysis of Cracks Handbook, Del Research Corp., Hellertown, Pennsylvania (1973).

[5] G. C. Sih, Handbook of Stress Intensity Factors for Researchers and Engineers, Institute of Fracture an Solid Mechanics, Lehigh University, Bethlehem, Pennsylvania (1973).

[6] 1974 Annual Book of ASTM Standards, Part 10 ASTM, Philadelphia (1974), p. 432.

[7] G. R. Irwin, in: Proceedings Seventh Sagamore Ordinance Materials Research Conference, Syracuse University Press, Syracuse, New York (1960), p. IV-63.

[8] G. R. Irwin, Trans. ASME, J. Basic Eng. 82, 1960, p. 417.

[9] P. C. Paris and G. C. Sih, in: Fracture Toughness Testing and Its Applications, ASTM STP 381, 1965, p. 30.

[10] A. A. Wells, Brit. Welding J., 12, 1965, p. 2.

[11] A. A. Wells, Brit. Welding J., 10 (11), 1963, p. 563.

[12] F. M. Burdekin and D. W. Stone, J. Strain Anal., 1966.

[13] D. S. Dugdale, J. Mech. Phys. Solids, 8 (2), 1960, p. 100.

[14] A. A. Wells, Congress of Applied Mechanics, Calgary, 1971, p. 57.

[15] F. M. Burdekin and M. G. Dawes, Proc. Mech. Eng. Conf., London, May 1971.

[16] M. G. Dawes, Advances in Elasto-Plastic Fracture Mechanics, edited by E. H. Larsson, Applied Science Publishers, London, 1980, p. 279.

[17] British Standard 5762: Methods for Crack Opening Displacement (COD) Testing, 1979, The British Standards Institution, London.

[18] J. R. Rice, J. Appl. Mech., 35 (2), 1968, p. 379.

[19] J. A. Begley and J. D. Landes, ASTM STP 514, 1972, p. 1.

[20] D. J. Hayes, Ph.D. Thesis, University of London, 1970.

[21] J. G. Blavel, Advances in Elasto-Plastic Fracture Mechanics, edited by E. H. Larsson, Applied Science Publishers, London, 1980, p. 65.

[22] M. G. Dawes, ASTM STP 668, 1979, p. 307.

[23] A. B. Stuber, Ph.D. Thesis, University of Kansas, 1980.

[24] R. O. Ritchie, R. F. Smith, and J. F. Knott, Metal Science, 9, 1975, p. 485.

[25] A. Penelon, M. N. Bassim, and J. M. Dorlot, ASTM STP 677, 1979, p. 449.

[26] I. Milne, Mat. Sci. Eng., 30, 1977, p. 243.

[27] G. G. Chell and G. M. Spink, Eng. Frac. Mech., 9, 1977, p. 101.

[28] I. Milne and P. J. Worthington, Mat. Sci. Eng., 26, 1976, p. 185.
[29] J. D. Landes, and J. A. Begley, ASTM STP 632, 1978, p. 57.
[30] W. Weibull, J. Appl. Mech., 18, 1953.
[31] I. H. Lin, Unpublished work.
[32] R. O. Ritchie, J. F. Knott, and J. R. Rice, J. Mech. Phys. Solids, 21, 1973, p. 395.
[33] G. G. Chell and A. Davidson, Mat. Sci. Eng., 24, 1976, p. 45.
[34] G. G. Chell and R. S. Gates, Int. J. Fract., 14 (2), 1978, p. 223.
[35] P. M. S. T. deCastro, J. Spurrier, and P. Hancock, ASTM STP 677, 1979, p. 486.
[36] M. G. Dawes, Private communication.

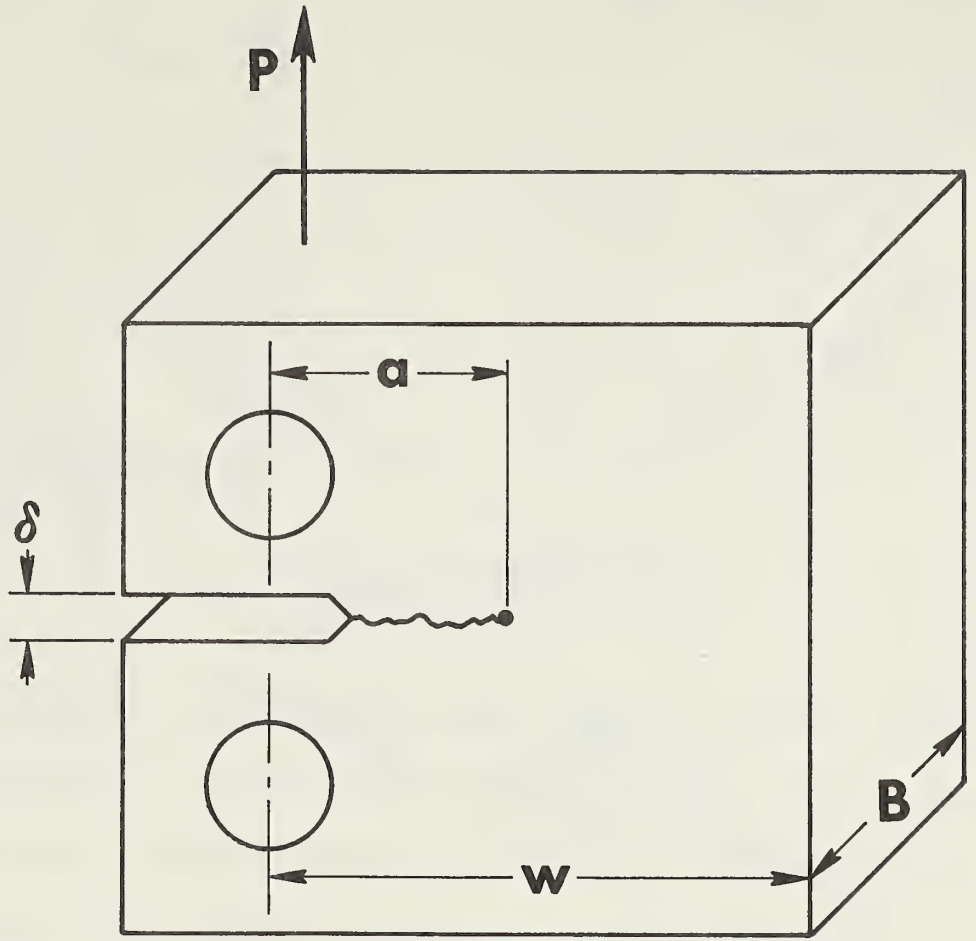

Fig. A1. ASTM E-399 compact specimen for fracture toughness testing.

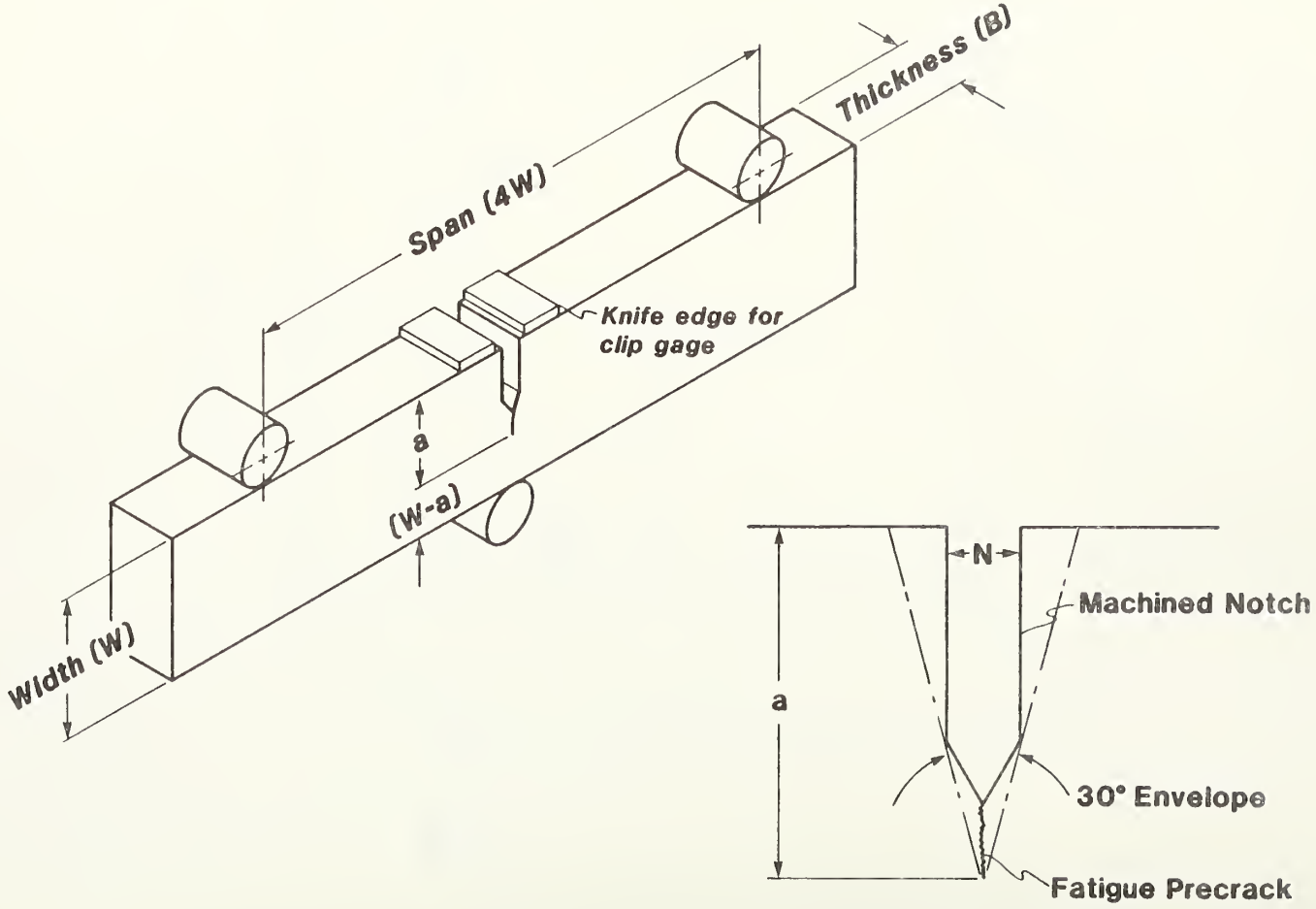

Fig. A2. Three-point bend specimen used to obtain CTOD test results.

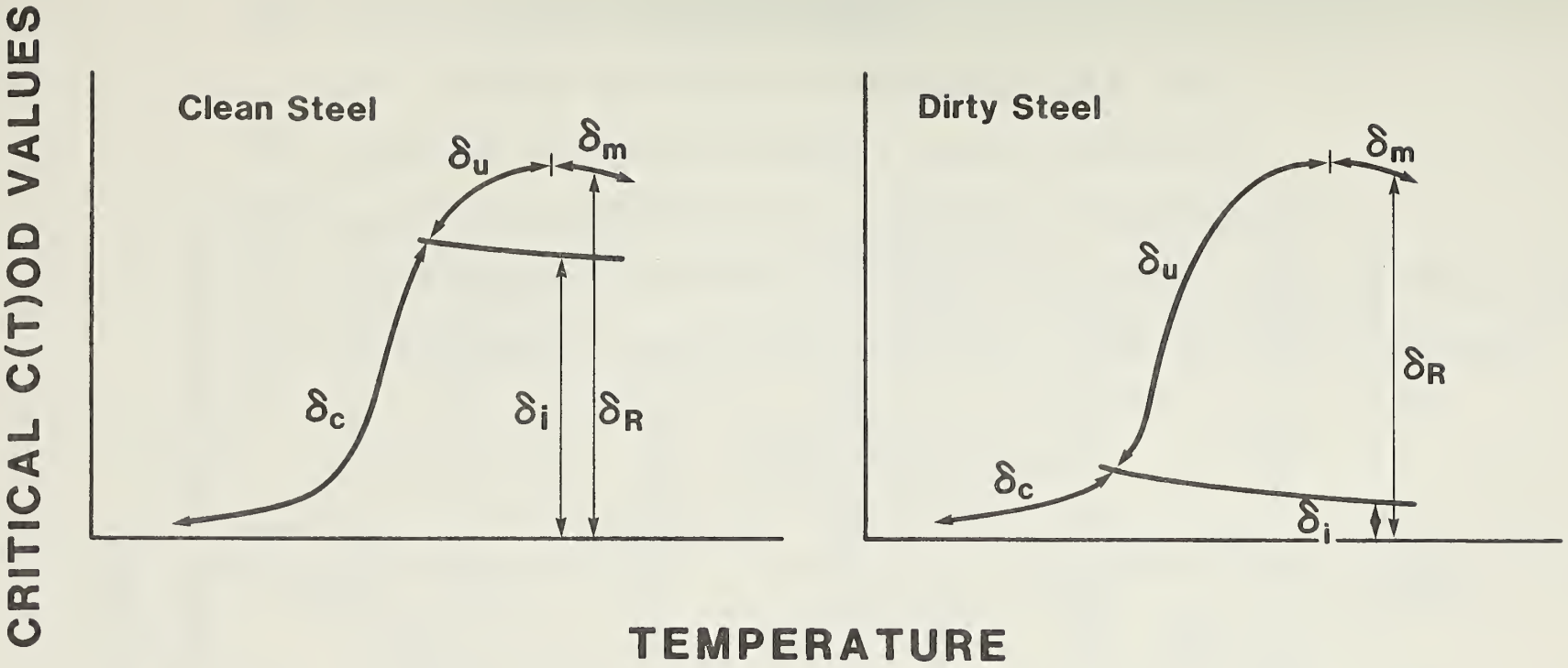

δ_c = Unstable cleavage-no prior slow crack growth

δ_u = Unstable cleavage-with prior slow crack growth

δ_m = Plastic collapse or tearing instability

δ_i = Onset of slow stable crack growth

δ_R = Resistance curve value

Fig. A3. Notation for critical CTOD values.

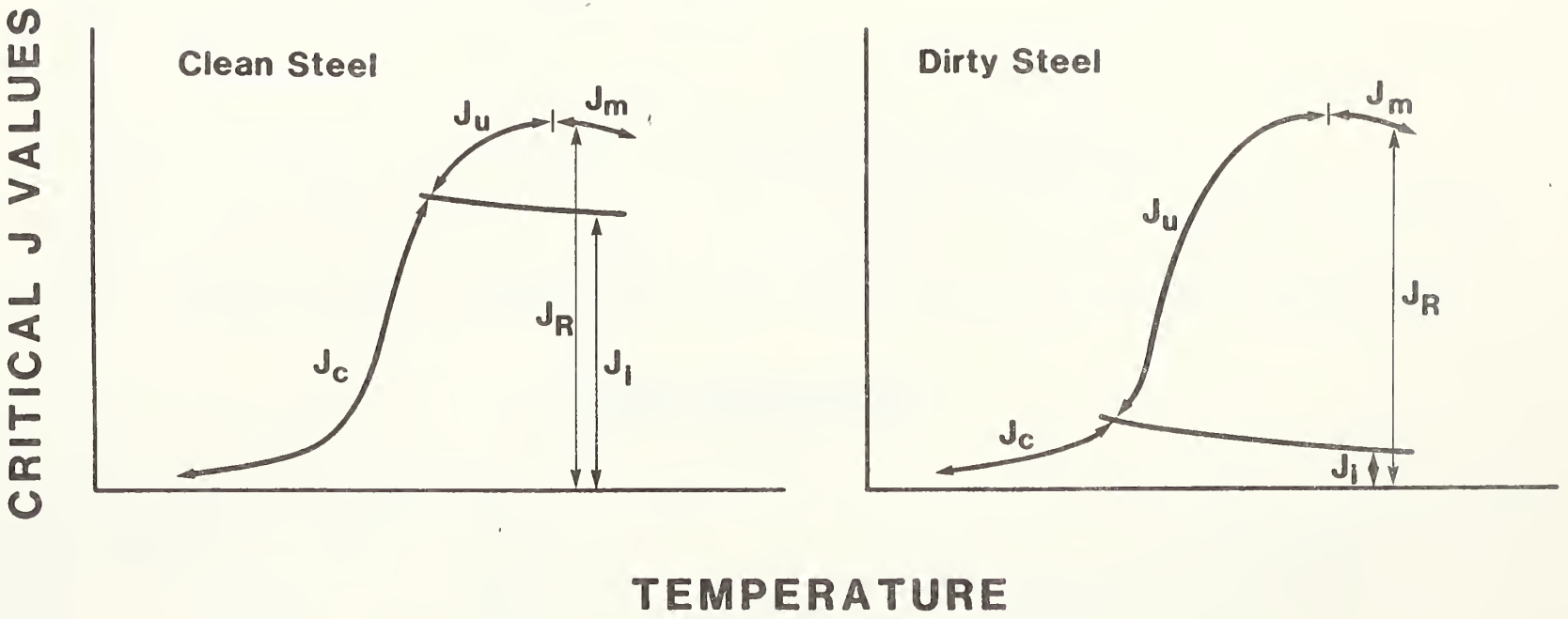

J_c = Unstable cleavage-no prior slow crack growth

J_u = Unstable cleavage-with prior slow crack growth

J_m = Plastic collapse or tearing instability

J_i = Onset of slow stable crack growth

= J_{Ic} when certain conditions are met

J_R = Resistance curve value

Fig. A4. Notation for critical J values.

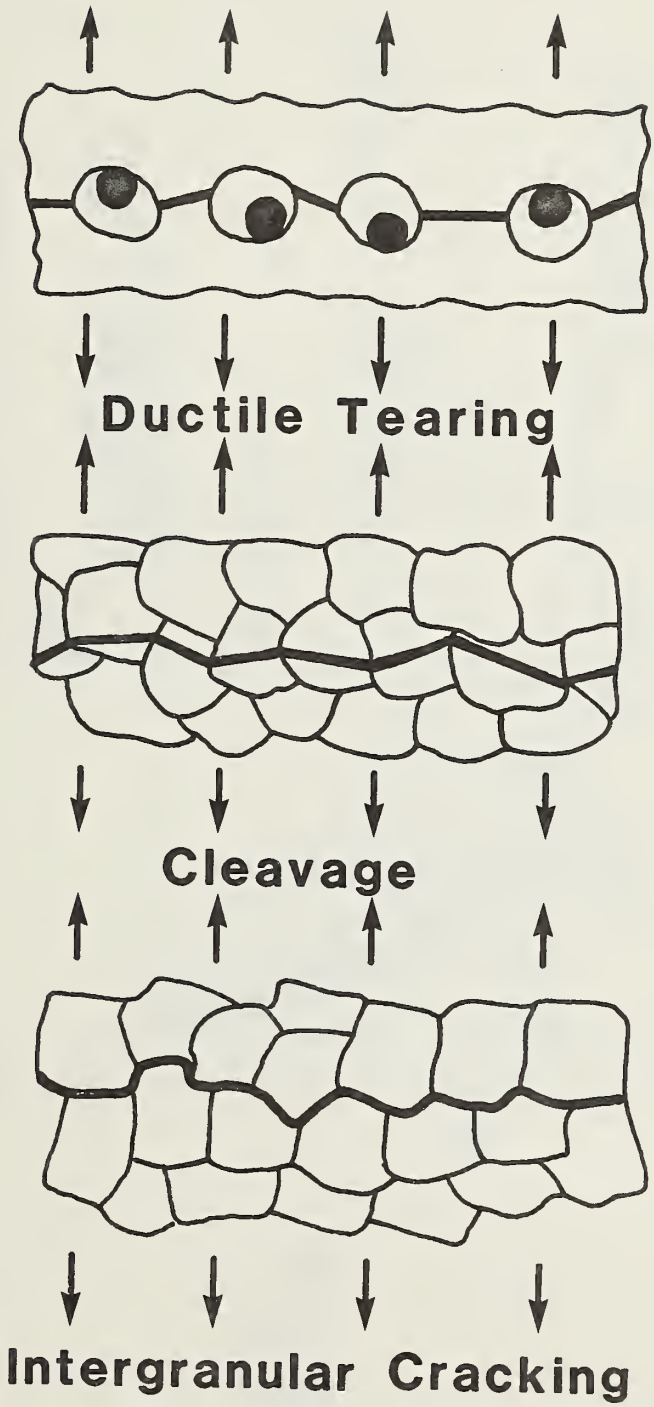

Fig. A5. The three basic micromechanisms of fracture.

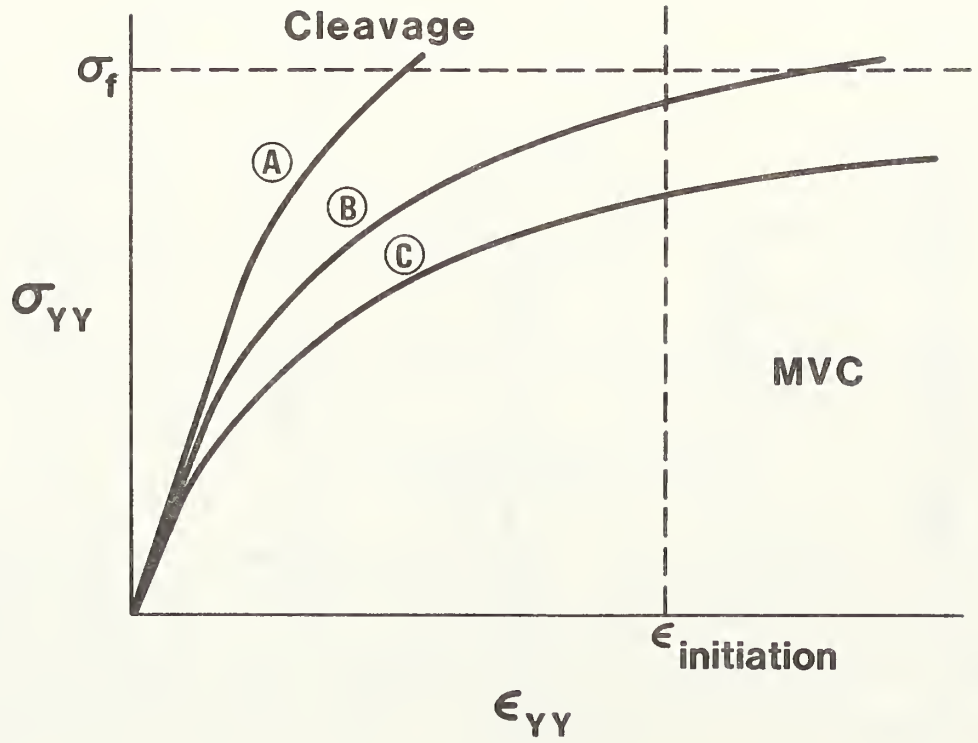

Fig. A6. Schematic representation of possible flow curves for material near the crack tip, illustrating the effect of flow stress on the micromechanism of fracture. (a) Cleavage, (b) cleavage preceded by ductile tearing, and (c) stable crack growth.

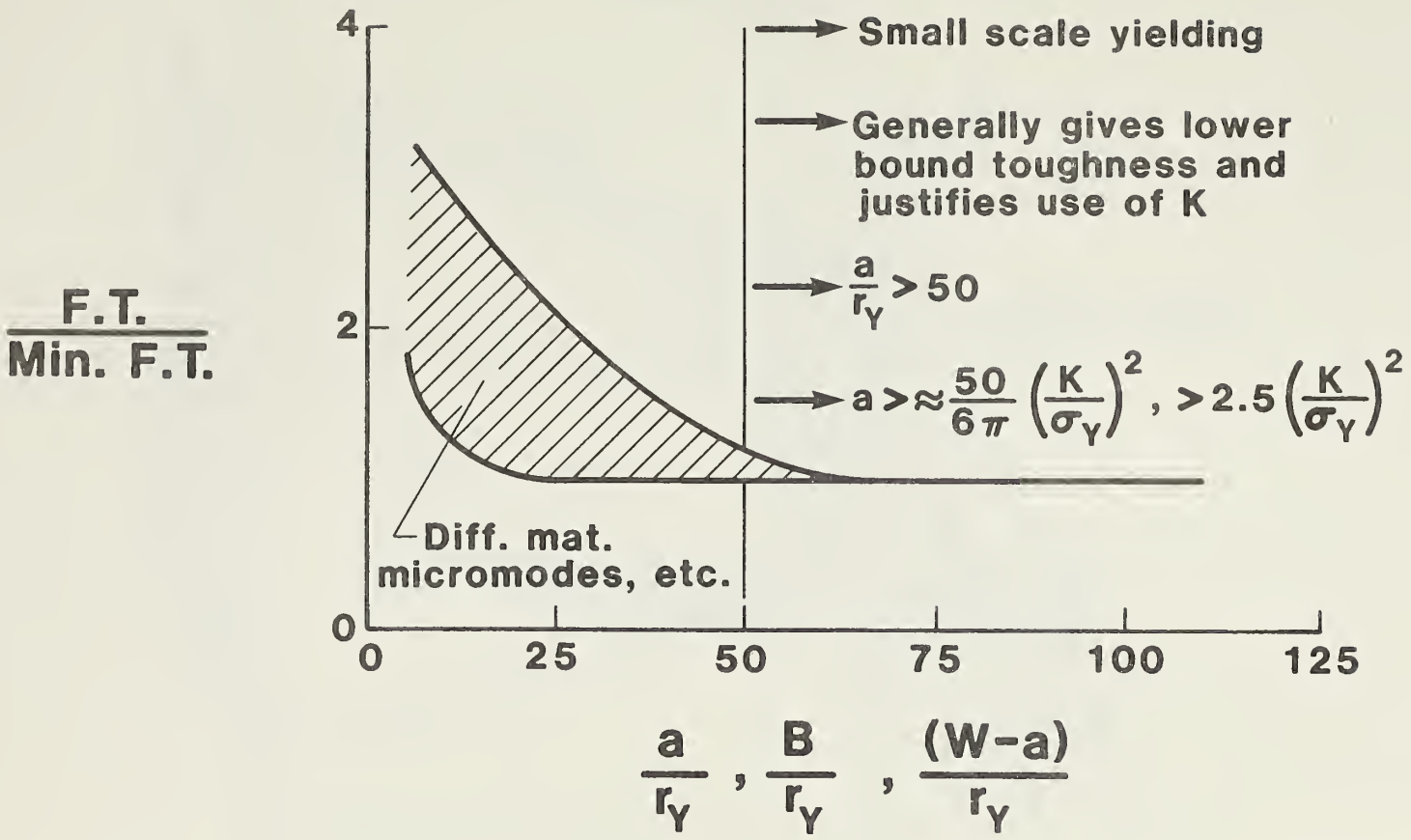

Fig. A7. Effect of specimen geometry and plastic zone size on fracture toughness. Specimens must lie to the right of the vertical line to meet ASTM E-399 specifications.

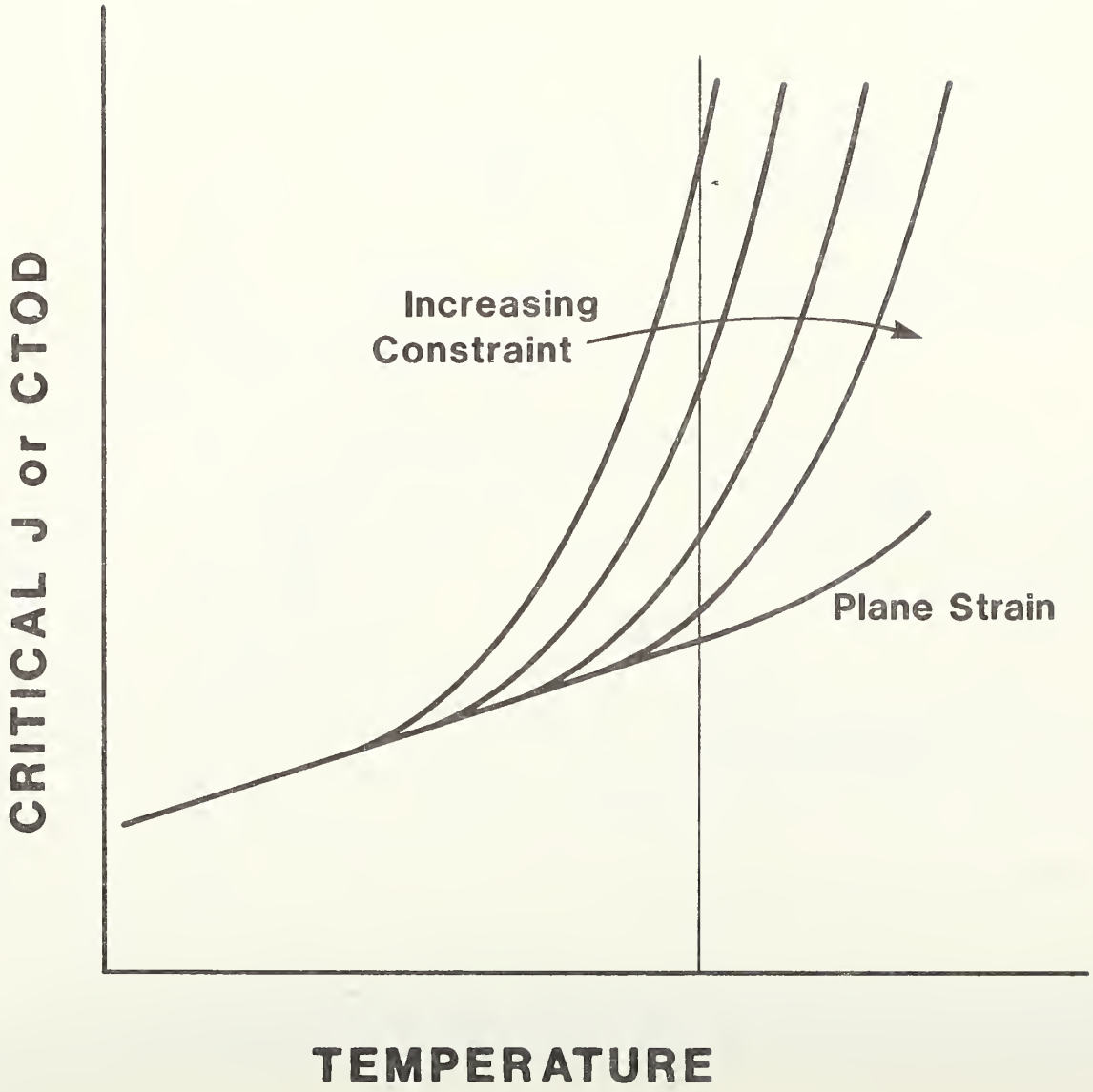

Fig. A8. Effect of constraint on ductile-to-brittle transition behavior.

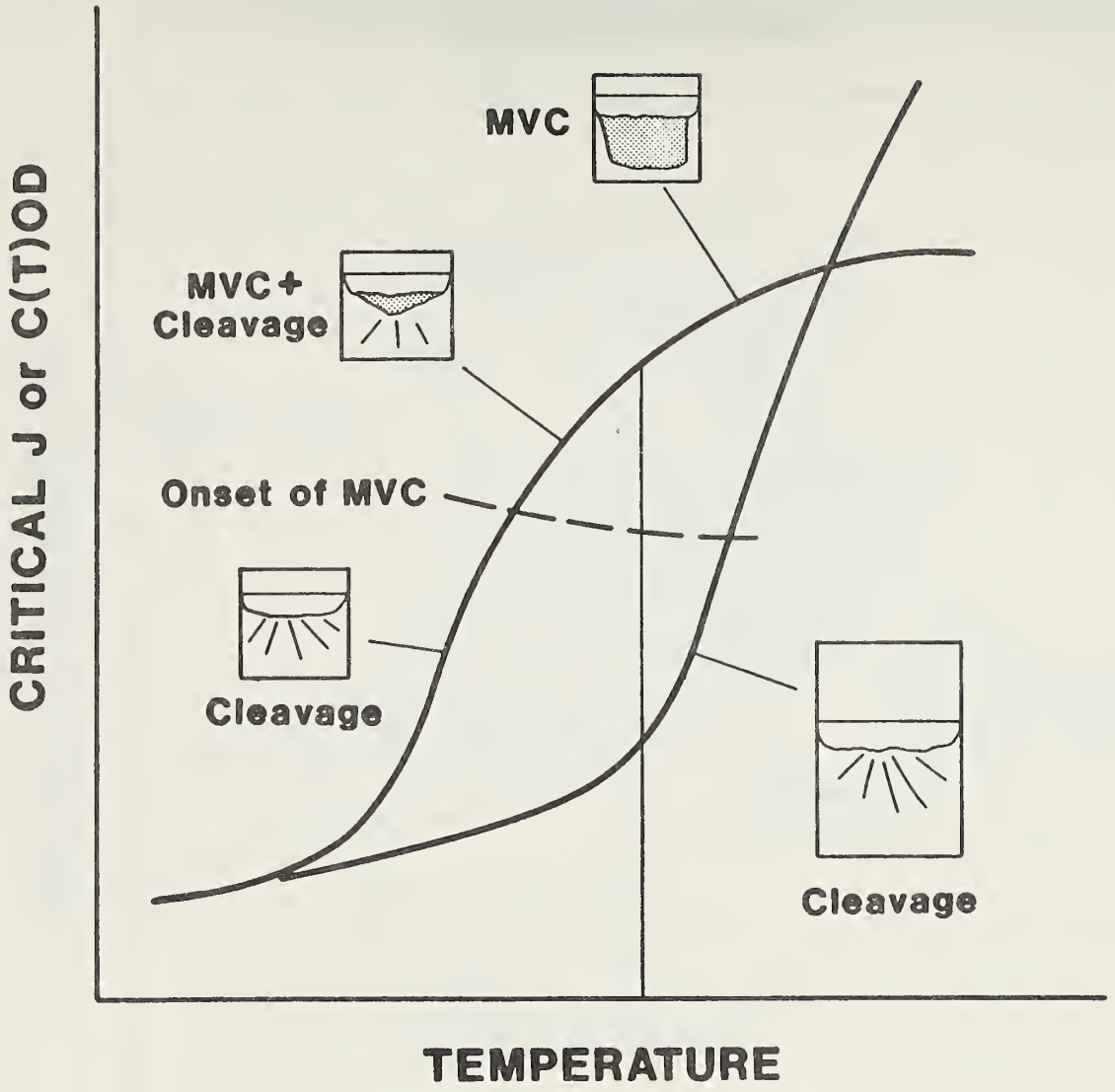

Fig. A9. Effect of constraint on the micromechanism of fracture. At the temperature represented by the vertical line the low constraint specimen fails by ductile tearing while the high constraint specimen fails by cleavage.

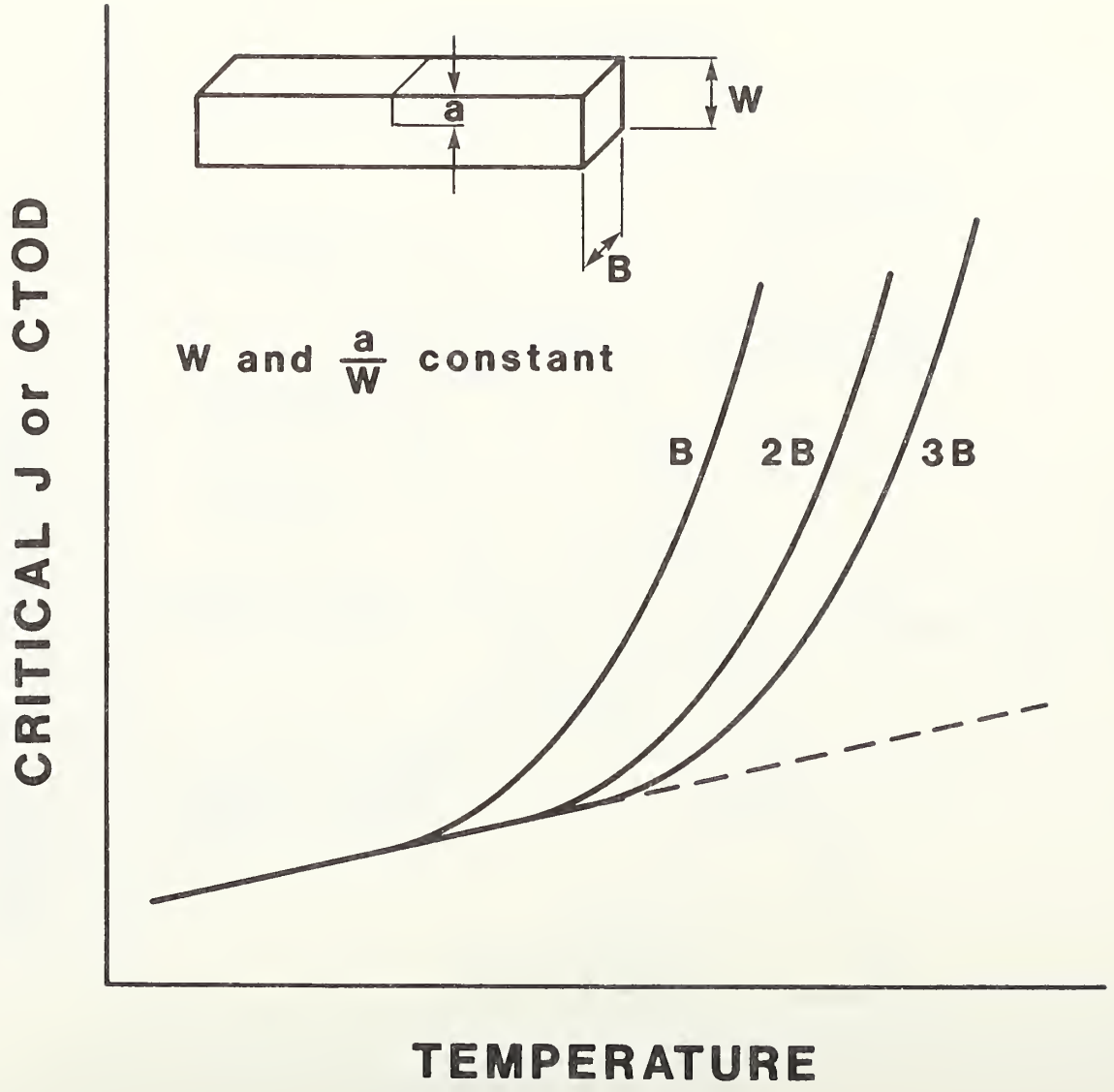

Fig. A10. Effect of specimen thickness on the ductile-to-brittle transition behavior.

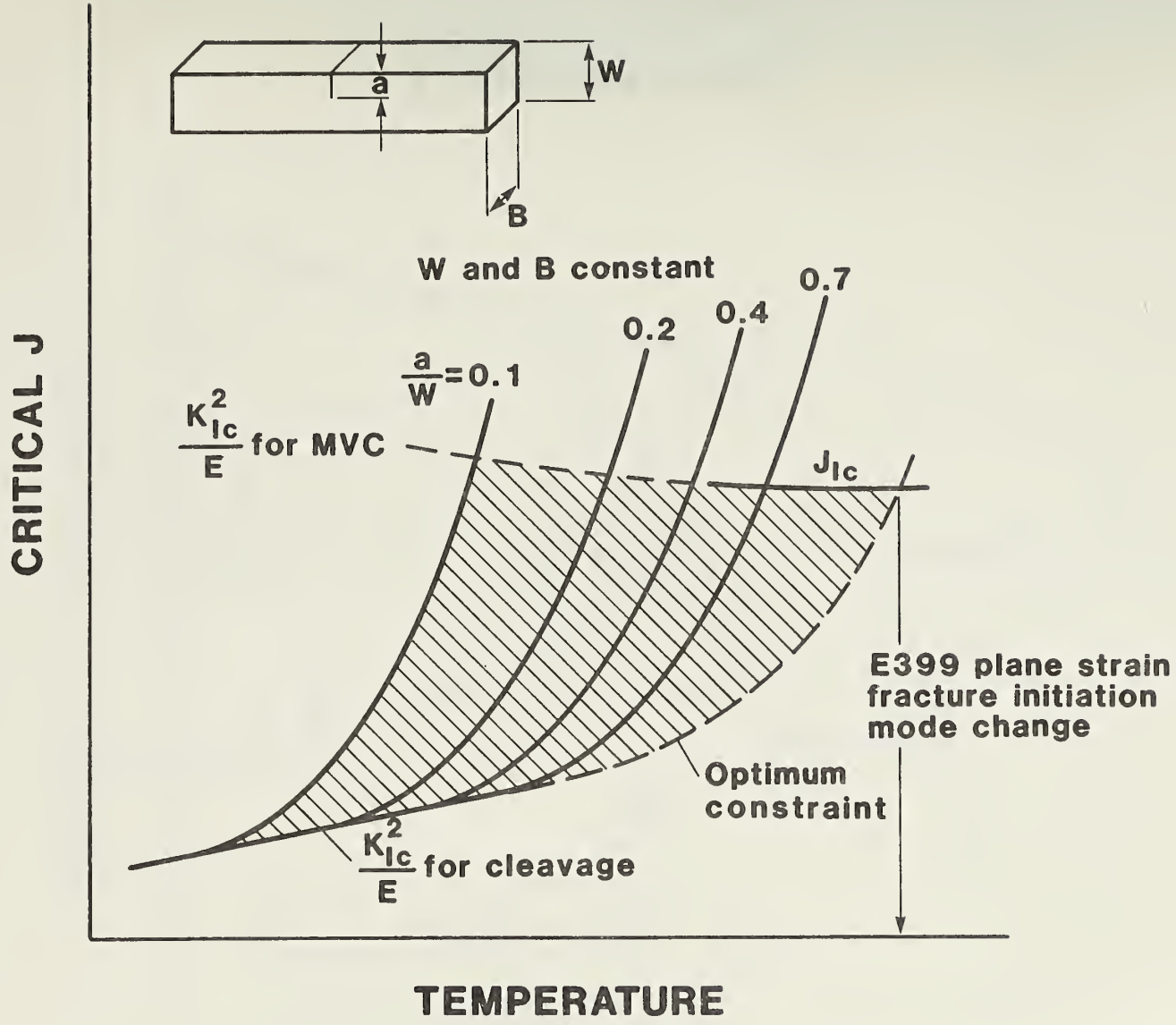

Fig. A11. Effect of notch depth on fracture behavior of SENB specimens.

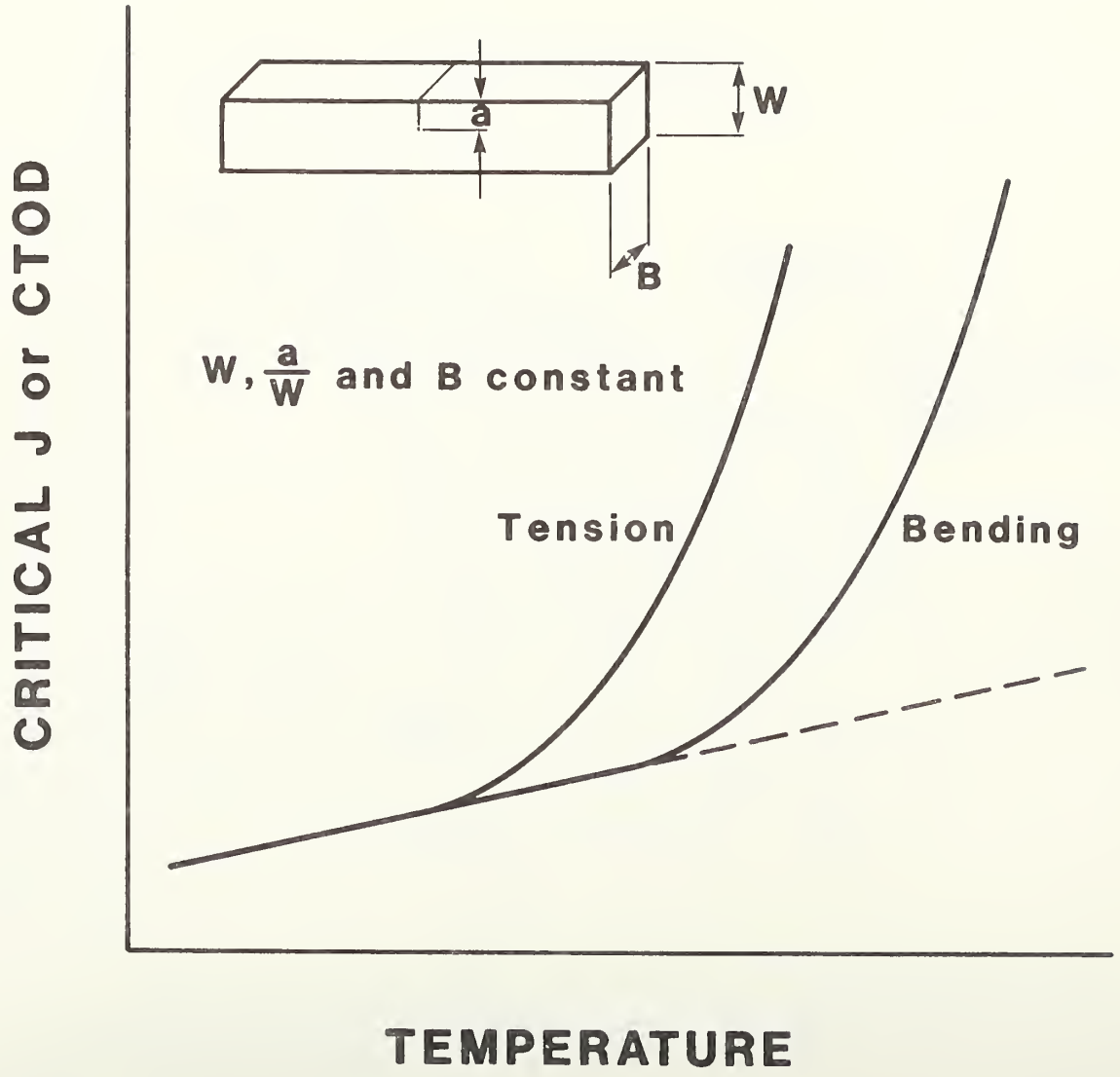

Fig. A12. Effect of type of loading on fracture toughness.

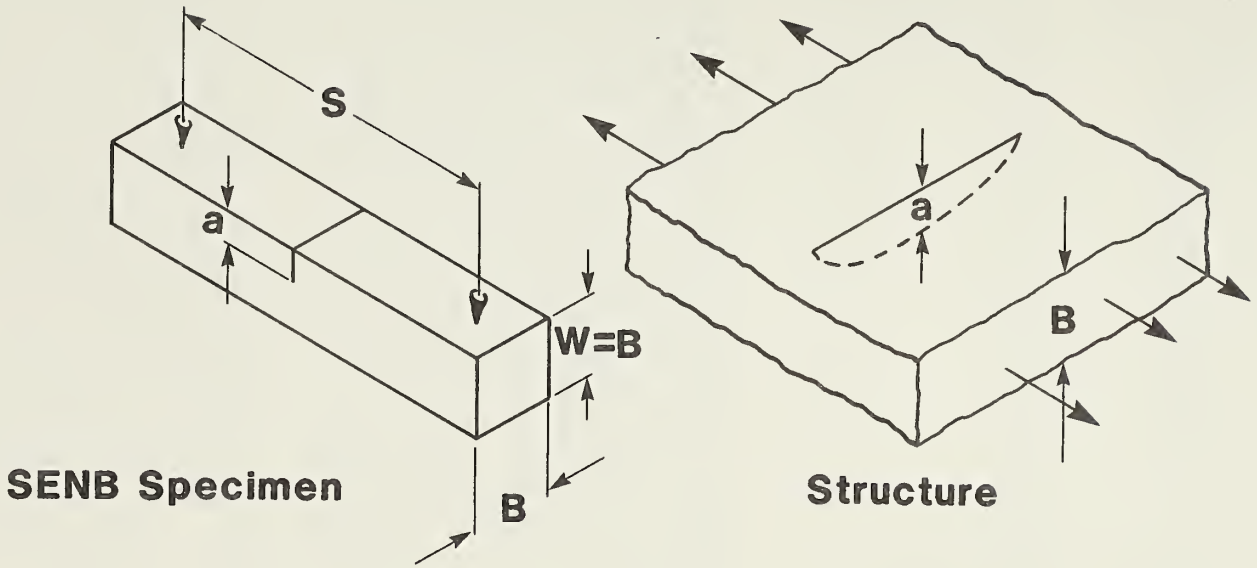

Fig. A13. Attempt to match the crack-tip region constraint (CTRC) of a structure with an SENB specimen.

NBS-114A (REV. 2-8C)

U.S. DEPT. OF COMM. BIBLIOGRAPHIC DATA SHEET (See instructions)	1. PUBLICATION OR REPORT NO. NBSIR 83-1680	2. Performing Organ. Report No.	3. Publication Date December 1982

4. TITLE AND SUBTITLE

Interim Progress Report:
FRACTURE TOUGHNESS OF STEEL WELDMENTS FOR ARCTIC STRUCTURES

5. AUTHOR(S)

T. L. Anderson and H. I. McHenry

6. PERFORMING ORGANIZATION (If joint or other than NBS, see instructions)

NATIONAL BUREAU OF STANDARDS
DEPARTMENT OF COMMERCE
WASHINGTON, D.C. 20234

7. Contract/Grant No.

8. Type of Report & Period Covered

9. SPONSORING ORGANIZATION NAME AND COMPLETE ADDRESS (Street, City, State, ZIP)

U.S. Department of Interior
Minerals Management Service
12203 Sunrise Valley Drive
Reston, VA 22091

10. SUPPLEMENTARY NOTES

☐ Document describes a computer program; SF-185, FIPS Software Summary, is attached.

11. ABSTRACT (A 200-word or less factual summary of most significant information. If document includes a significant bibliography or literature survey, mention it here)

This report summarizes the progress in the development of fracture criteria for steel weldments in arctic structures. Tensile, Charpy-impact, and fracture toughness properties have been measured as a function of temperature for a 25.4 mm (1 in) thick plate of normalized steel. Fracture toughness tests were performed on five geometries of single-edge notched bend (SENB) specimens. Critical values of the J-integral and the crack-tip opening displacement (CTOD) were computed and plotted versus temperature. The ductile-to-brittle transition temperature increased with increasing specimen thickness, and crack length. The effect of specimen geometry on fracture toughness is attributed to changes in crack-tip region constraint with geometry. Initial attempts to model this behavior have been moderately succesful.

Various aspects of the SENB fracture toughness test are being examined. Preliminary results indicate that the J-integral can be accurately measured with either load-line displacement or mouth-opening displacement measurements. It may therefore be possible to measure both J and CTOD with a single clip gage. The relationship between J and CTOD has been investigated. The ratio of J to CTOD is a function of yield strength, displacement and work-hardening rate. The eta factor, which is a dimensionless constant used to relate the J-integral to energy absorbed by the specimen, was found to be independent of crack length for SENB specimens with a/W ranging from 0.19 to 0.75.

12. KEY WORDS (Six to twelve entries; alphabetical order; capitalize only proper names; and separate key words by semicolons)

arctic structures; crack-tip opening displacement; ductile-to-brittle transition; elastic-plastic fracture; J-integral; mechanical properties; structural steels; toughness.

13. AVAILABILITY

☒ Unlimited
☐ For Official Distribution. Do Not Release to NTIS
☐ Order From Superintendent of Documents, U.S. Government Printing Office, Washington, D.C. 20402.
☒ Order From National Technical Information Service (NTIS), Springfield, VA. 22161

14. NO. OF PRINTED PAGES 86

15. Price $10.50

INSTRUCTIONS

FORM NBS-114A: BIBLIOGRAPHIC DATA SHEET. This bibliographic data sheet meets the standards adopted for use by all U.S. Government agencies. It is needed for NTIS processing and must accompany all NBS papers, those appearing in nongovernmental media as well as those in NBS series, since all reports of NBS technical work are normally entered into the NTIS system. For all GPO publications, it becomes an integral part of the document and is widely used by librarians and abstractors.

Items 1, 2 – Complete if information is available; otherwise Publications Office will complete later. If non-NBS publication, state "see item 10" (Enter other agency sponsor's report number if requested to do so, and enter NBSIR number under item 2).

Item 3 – Complete if known; otherwise Publications Office will complete.

Items 4, 5 – Complete as shown on manuscript. When NBS-114A is resubmitted along with NBS-266, following publication of non-NBS media papers, these items must agree with published paper.

Item 6 – If not NBS, blank out and enter Grantee/Contractor name and address, or if performed jointly, show both.

Item 7 – Complete when applicable.

Item 8 – Enter "Interim," "Final," or period covered.

Item 9 – Enter all sponsors' names and addresses. Include NBS if also a sponsor.

Item 10 – Enter other relevant information, i.e., related or superseded documents. Also used by Publications Office for Library of Congress catalog number, and entry of non-NBS media citation upon receipt of Form NBS-266 from author. Check block if appropriate and attach SF185.

Item 11, 12 – Prepare abstract and key words with special care. These are published separately by NBS, NTIS, and other bibliographic services, and are vital elements in guiding readers to your paper. The key words will be used as entries in a subject index. See NBS Communications Manual for additional guidance.

Item 13 – Indicate "Unlimited" – for open-literature documents cleared under NBS editorial procedures, or "For official distribution. Do not release to NTIS" – for limited, restricted, or need-to-know material (See Communications Manual). Publications Office will mark appropriate "order" box and complete Stock Number when known.

Items 14, 15 – Leave blank. To be completed by Publications Office or call Printing and Duplicating for NBSIR's.


AMERICAN BINDERY - EAST
1993